land

MDPI

Article

An Analysis of Land Use Conflicts and Strategies in the Harbin–Changchun Urban Agglomeration Based on the Production–Ecological–Living Space Theory and Patch-Generating Land Use Simulation

Xiaomeng Wang, Yanjun Zhang *, Xiaoyan Li and Shuwen Cao

College of Earth Sciences, Jilin University, Changchun 130061, China; wangxm23@mails.jlu.edu.cn (X.W.); lxyan@jlu.edu.cn (X.L.); caosw23@mails.jlu.edu.cn (S.C.)
* Correspondence: yanjunzhang@jlu.edu.cn

Abstract: In recent years, rapid economic development, increasing human activities, and global climate change have led to escalating demands for land across production, residential, and ecological domains. This surge has heightened land use conflicts, significantly impacting sustainable land utilization and regional sustainable development. Drawing upon the "Production–Ecological–Living Space" (PELS) theory, this study employs a Patch-generating Land Use Simulation (PLUS) model to project the PELS of the Harbin–Changchun Urban Agglomeration (HCUA) under four scenarios for 2030. Introducing the concepts of absolute and relative conflicts in land use, this study utilizes a spatial comprehensive conflict index (SCCI) model to assess the progression of absolute conflicts from 2000 to 2020 and across various scenarios for 2030, while a remote sensing ecological index (RSEI) model is utilized to evaluate the evolution of relative conflicts from 2000 to 2020. The results indicate the following: (1) From 2000 to 2020 and different scenarios in 2030, the PELS of the HCUA is dominated by forest ecological space (E1) and agricultural production space (P1), with no substantial alterations in the overall spatial distribution of the PELS. (2) Absolute and relative conflicts between 2000 and 2020 are mainly concentrated in the plains of the western regions, characterized by conflicts arising from the encroachment of living space on production space; however, absolute conflicts have declined annually, accompanied by a notable enhancement in ecological quality. (3) The spatial pattern of absolute conflicts in 2030 exhibits minimal variation, illustrating higher values in the western regions compared to the eastern parts, with living space surpassing ecological space and plains showing higher conflict values than mountains. Notably, the economic development (ED) scenario exhibits the most intense conflicts, with areas of high conflict prevailing, whereas the sustainable development goals (SDGs) scenario depicts enhancements in absolute conflicts while maintaining equilibrium between economic and ecological development requirements. This research offers valuable insights into mitigating land use conflicts in the HCUA, provides a new perspective for studying changes in land use conflicts, and serves as a scientific reference for sustainable land utilization and regional sustainable development.

Keywords: Production–Ecological–Living Space (PELS); absolute conflict; relative conflict; Patch-generating Land Use Simulation (PLUS); remote sensing ecological index (RSEI); Harbin–Changchun Urban Agglomeration (HCUA)

check for updates

Academic Editor: Dingde Xu

Received: 4 December 2024
Revised: 30 December 2024
Accepted: 6 January 2025
Published: 8 January 2025

Citation: Wang, X.; Zhang, Y.; Li, X.; Cao, S. An Analysis of Land Use Conflicts and Strategies in the Harbin–Changchun Urban Agglomeration Based on the Production–Ecological–Living Space Theory and Patch-Generating Land Use Simulation. *Land* **2025**, *14*, 111. https://doi.org/10.3390/land14010111

Copyright: © 2025 by the authors. Licensee MDPI, Basel, Switzerland. This article is an open access article distributed under the terms and conditions of the Creative Commons Attribution (CC BY) license (https://creativecommons.org/licenses/by/4.0/).

1. Introduction

Based on the data from China's 7th National Population Census, the national urbanization rate surged to 63.89% by 2020, exceeding the global average and marking a 45.97% increase from 1978 [1]. The urbanization rates in Heilongjiang Province and Jilin Province stood at 60.9% and 58.3%, respectively. Amid rapid urbanization, the intensive development and utilization of land resources have engendered critical challenges, including resource constraints and heightened land use conflicts [2]. Furthermore, the profound impacts of intense human activities and global environmental changes have reverberated across the global terrestrial system [3]. These impacts are notably evidenced in alterations in land use and land cover, characterized by urban sprawl, agricultural expansion, cultivated land loss, deforestation, and grassland degradation. Rapid changes in land use have disrupted the equilibrium in the "Production–Ecological–Living Space" (PELS) [4], resulting in escalating conflicts among production, residential, and ecological spaces. The competition for national territorial space has intensified, amplifying conflicts between human activities and natural environments, production and residential areas, and various ecosystems. Land use conflicts, as a prominent manifestation of intensified human activities and drastic global climate change, impede the sustainable management of land resources and pose a substantial challenge to the sustainable development of national territories [5,6]. Given that intense land use conflicts often coexist with discordant human–environment interactions, they pose a threat to ecosystem health and environmental quality [7]. Consequently, the pursuit of balanced development in the PELS to address escalating land use conflicts has become a crucial focal point in land science research [2,4,8].

Land use conflicts refer to the process of spatial competition and negotiation among various land use entities and stakeholders in pursuit of divergent objectives [5,9,10]. This phenomenon primarily arises from the scarcity of land resources and expanding and diverse human needs, resulting in situations where land use within a specific timeframe and region fails to meet the diverse demands for products and services [3]. This mismatch leads to imbalances, resulting in land use conflicts [11,12]. The PELS theory is rooted in the "element–structure–function" paradigm of system theory [13,14], where production, living, and ecological spaces encompass the spectrum of spatial activities spanning material production and spiritual well-being. The fundamental cause of PELS conflicts stems from limited spatial resources and the insatiable demand for societal advancement [15]. The examination of PELS conflicts aligns closely with the study of land use conflicts, albeit with a nuanced difference: PELS provides a more comprehensive and high-level reflection of the intricate characteristics of various land use types, distinguishing it from the concrete spatial occurrence represented by land use conflicts [16]. Over time, government macro-control has achieved significant success in allocating construction land resources; however, this has simultaneously exacerbated PELS conflicts. For instance, the encroachment of living space into agricultural production space and industrial space into ecological space has impeded the harmonious development of the PELS [2].

In response to these challenges, the academic community is increasingly focusing on achieving a delicate balance among the fundamental objectives of food security, economic growth, and sustainable development within territorial spatial planning. The aim is to facilitate the high-quality advancement of territorial space and establish a symbiotic relationship between humanity and the landscape [2]. Initiatives ranging from the inception of the IGBP (International Geosphere-Biosphere Program) to the IHDP (International Human Dimensions Programme on Global Environmental Change), along with the evolution of LUCC (Land Use/Land Cover Change) and the GLP (Global Land Programme), have brought about a heightened awareness of issues such as land use conflicts, land resource monitoring through remote sensing, and future scenario forecasting [17–20]. With ad-

vancements in remote sensing technology and big data, novel opportunities have emerged for gathering land use and land cover information across diverse spatial and temporal scales, enriching our comprehension of the spatiotemporal dynamics of land use conflicts. Additionally, to foster global human well-being and promote natural resource conservation, the United Nations introduced the transformative "Transforming Our World: The 2030 Agenda for Sustainable Development" (referred to as the "Agenda") in 2015. Described as a comprehensive "plan of action for people, planet, and prosperity", the "Agenda" comprises 17 sustainable development goals (SDGs), 169 specific targets, and 231 unique indicators [21]. This framework is designed to address the challenges posed by increasing population and consumption patterns, with a primary focus on various dimensions of sustainability that resonate with the global development community [22]. Each goal, whether directly or indirectly related, is geared towards enhancing human well-being and encapsulates the integrated and sustainable progress of societal advancement, economic growth, and environmental stewardship [23]. Given the constrained land area and diverse land requisites of the HCUA, the selection of appropriate SDGs is pivotal for realizing the harmonized development of the PELS.

In recent years, scholars from both domestic and international arenas have made significant strides in researching conflicts within the PELS from diverse perspectives, utilizing varied research methods and focusing on a range of research subjects. The research landscape has continually evolved, emphasizing the measurement and categorization of different types of PELS conflicts [24–27], the spatiotemporal dynamics of PELS conflicts [4,28–30], future scenario predictions of conflicts [8,31,32], and conflict optimization and regulation [33,34]. Among these aspects, the accurate identification of PELS conflicts is the foundation of conflict research and the key to subsequent studies [2]. The scope of research has expanded and improved consistently, encompassing macro regions such as urban agglomerations [31,35–37], river basins [38,39], and provinces [40,41], alongside micro regions like cities [42], counties [43], and even special zones like mines [33] and islands [27]. Research methodologies have gradually transitioned from qualitative to quantitative approaches. Initially, qualitative methods like participatory surveys [16] and game theory [44] are prevalent, underscoring the social dimensions of land use conflicts, albeit relying heavily on extended questionnaires and lacking the quantification of conflict intensity. With advancements in 3S technology, abundant spatial data have offered geographical insights into land use conflicts, driving a shift towards quantification. The main methods include the use of a Pressure–State–Response (PSR) model, multi-objective evaluation, and landscape ecological risk assessment. While the PSR model provides a comprehensive assessment of conflict intensity within a study area, it may face challenges in segmenting conflict levels and delineating spatial conflict domains [43]. Multi-objective evaluation can identify plots suitable for multiple land use types, identifying potential conflict spaces, but the selection of evaluation indicators is subjective, requiring scientific and reasonable choices based on specific situations [45].

The landscape ecological risk assessment method (i.e., SCCI model) is mainly based on the landscape pattern perspective, using the complexity index of land use to represent the sources of landscape ecological risks. The fragility index of land use characterizes the receptors of landscape ecological risks, while the stability index of land use reflects the effects of landscape ecological risks. Subsequently, a comprehensive measurement model of spatial conflicts is constructed to achieve the purpose of measuring conflicts in the PELS [46]. The evaluation dimensions of PELS conflicts can correspond to the content of landscape ecological risk assessment [17]. This method typically uses grids as conflict assessment units to evaluate the levels and spatial distribution characteristics of PELS conflicts, which is more accurate in identifying conflict locations. By using relatively

objective landscape pattern indices to construct the measurement model, subjectivity in selecting evaluation criteria is effectively avoided. Therefore, this method has been widely applied in the identification of spatial conflicts and intensity diagnosis. Currently, many scholars use the SCCI model for conflict estimation. For example, Meimei Wang utilized the SCCI model to study the absolute land use conflicts in the Xining urban area [8]. Qingping Lu used the SCCI model to assess the PELS conflicts in different geomorphic types of mountain–basin areas in the karst regions of China [47]. Qian Zuo used this method to study land use conflicts in the central mountainous regions of China [48]. The research scale covers macro, micro, and special regions. In conclusion, accurately quantifying the spatiotemporal characteristics of PELS conflicts and understanding their impact on land use dynamics are essential for promoting the equilibrium between regional development and the sustainable utilization of land resources.

Most existing studies predominantly focus on absolute conflicts within the framework of the PELS, while relatively little attention is given to addressing relative conflicts. This study categorizes PELS conflicts into two distinct types: absolute conflicts and relative conflicts. Absolute conflicts refer to the phenomenon of spatial competition and rights conflicts between people and land use patterns and structures generated by stakeholders in the process of land resource utilization. Relative conflicts necessitate an assessment of the dynamic changes in conflicts during a certain period of time to reflect the intensification or weakening of conflicts in a certain spatial area during a certain period of time. Absolute conflicts are characterized by conflict values calculated based on intrinsic land features, such as fragmentation and patch count [49]. The primary aim of absolute conflicts is to visualize the extent and distribution of conflicts across the entire region [8]. In contrast, relative conflicts, utilizing the remote sensing ecological index (RSEI), primarily analyze comparative differences over different time periods. From the perspective of ecological responses, they identify and measure areas with significant changes in land use conflicts, offering a more nuanced representation of relative conflict levels within the PELS [43,50]. While the academic community has extensively developed a comprehensive measurement system and a unified understanding of absolute conflict [8], research on relative conflicts remains limited. Meimei Wang employed the Pythagorean Fuzzy Conflict Information (PFCI) system to assess competition for various land types between core and peripheral areas, incorporating the competition for land resources across different administrative units (relative space) [8]. Similarly, Deling Wang focused on comparing different years to identify and measure areas with significant changes in land use conflicts from an ecological response perspective, thereby elucidating relative conflict levels (relative time) [43]. Consequently, there exists a necessity to propose a viable quantitative framework for assessing relative conflict levels.

This study leverages the existing research of scholars in the field of PELS conflicts, with a specific focus on the HCUA. It employs an objective valuation method utilizing the remote sensing ecological index (RSEI) to assess the ecological environmental quality within the HCUA. A comprehensive analysis and evaluation of the ecological environmental quality are performed, leading to the development of a relative conflict measurement model for the PELS by integrating landscape pattern indices. This analytical framework holds potential applicability for investigating PELS conflicts in regions beyond China or internationally encountering spatial pressures due to rapid socio-economic growth. The aim of this study is to propose a quantitative approach, utilizing the HCUA as a case study, to probe into the relative conflicts within the PELS framework along with future scenario predictions and absolute conflict measurements. Revealing the evolutionary trajectory of conflicts within the PELS in the HCUA not only helps us understand the evolutionary process of land use

as a human–environment system but also has significant practical value for scientifically formulating land use plans and pursuing sustainable land management (Figure 1).

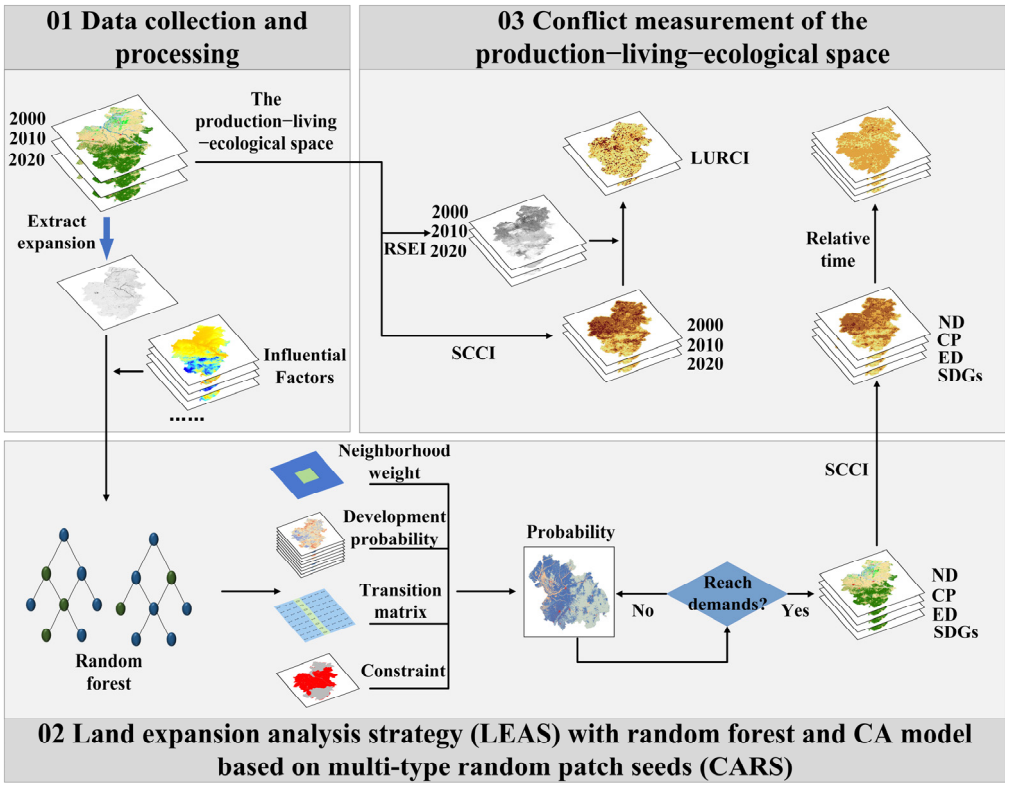


Figure 1. A flowchart of the proposed method.

2. Materials and Methods

2.1. Study Areas

The HCUA is a vital component of the urban agglomerations in Northeast China. It is located at the northern end of the Beijing–Harbin and Beijing–Guangzhou corridor, which is part of China's "two horizontal and three vertical" urbanization strategy. This urban agglomeration was established with the approval of the State Council against the backdrop of promoting the "Belt and Road" initiative, the revitalization of the Northeast's old industrial bases, and the deepening of new urbanization development. It holds a significant position in advancing new urbanization and expanding new space for regional development. Compared to other urban agglomerations selected in existing studies, the HCUA is an important old industrial base and the nation's primary grain production center [31]. Within its production space, the Sanjiang Plain and Songnen Plain offer abundant and fertile lands crucial for agricultural production and grain cultivation. As for its living space, the region has one mega-city, one Type I large city, four Type II large cities, and four medium-sized cities, forming a relatively complete urban system. In terms of ecological space, the HCUA houses numerous national forest parks, nature reserves, and strategic ecological zones.

The HCUA consists of 11 prefecture-level cities (or prefectures) from Heilongjiang Province and Jilin Province, including Harbin, Daqing, Qiqihar, Suihua, Mudanjiang, Changchun, Jilin, Siping, Liaoyuan, Songyuan, and the Yanbian Korean Autonomous Prefecture (Figure 2). In this composition, Harbin serves as a mega-city, Changchun as a Type I large city, and Daqing, Qiqihar, Jilin, and Siping as Type II large cities, while the others are medium-sized cities. The region boasts a well-established urban network and shows substantial growth potential. At the end of 2020, the HCUA spanned a land area of

322,547.53 square kilometers, housed an estimated permanent population of around 42.65 million, and recorded a total regional GDP of approximately CNY 535.17 billion in 2022.

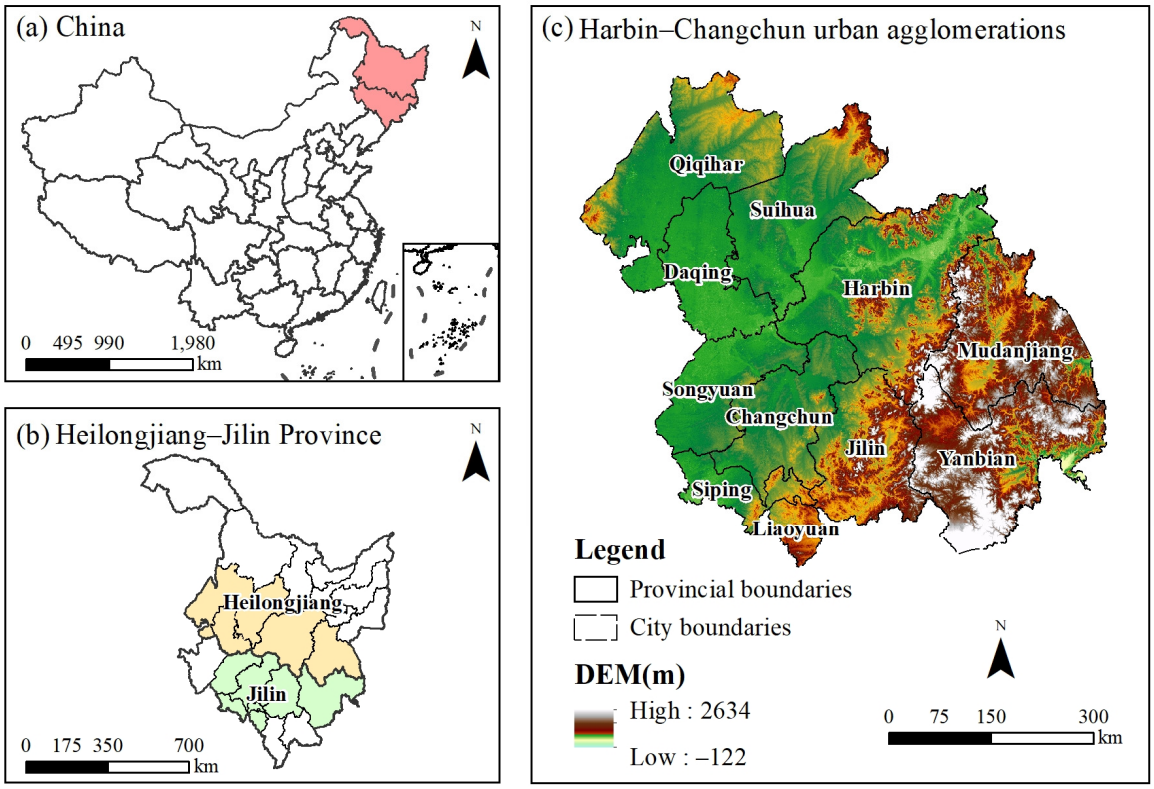


Figure 2. The spatial scope of the HCUA. (**a**) Heilongjiang–Jilin Province in China, (**b**) the HCUA in Heilongjiang–Jilin Province, and (**c**) the location and DEM map of the study area in 2020. Note: The base map is sourced from the Standard Map Service Network of the Ministry of Natural Resources (http://bzdt.ch.mnr.gov.cn/, accessed on 12 August 2024), with the survey number GS(2023)2767.

2.2. Data Sources

This study selected remote sensing images and land use data for the HCUA from 2000, 2010, and 2020 as the data foundation, focusing on the land use types in the PELS as the research object. By combining the SCCI model and RSEI, this study characterized the PELS absolute and relative conflicts of the HCUA.

The land use datasets from 2000, 2010, and 2020 originate from the Data Center for Resources and Environmental Sciences of the Chinese Academy of Sciences (https://www.resdc.cn/, accessed on 5 September 2024). These data are based on Landsat series satellite remote sensing images processed with ENVI 5.6 software. Manual interactive visual interpretation was conducted at a spatial resolution of 30 × 30 m to ensure data reliability. The remote sensing image data were obtained from the Geospatial Data Cloud (https://www.gscloud.cn/, accessed on 6 September 2024). After analysis and comparison, three Landsat remote sensing images from June 1 to September 30 of each year were selected for testing. Landsat 5 images were used for 2000 and 2010, whereas Landsat 7 images were used for 2020. The high-quality imagery of the study area met the precision requirements for research analysis.

The land use simulation data in this study mainly include a natural geographical dataset, socio-economic dataset, and development restriction dataset. Population and GDP data in the socio-economic dataset were acquired from the Data Center for Resources and Environmental Sciences of the Chinese Academy of Sciences, and the road system data originate from the National Catalogue Service for Geographic Information (https:

//www.webmap.cn/, accessed on 9 September 2024). Temperature and precipitation data in the natural condition dataset were also sourced from the Data Center for Resources and Environmental Sciences of the Chinese Academy of Sciences. Elevation and slope data were obtained from the Geospatial Data Cloud, and soil data were sourced from the Data Center for Resources and Environmental Sciences of the Chinese Academy of Sciences. In the development restriction dataset, ecological protection area data came from the Data Center for Resources and Environmental Sciences of the Chinese Academy of Sciences, and river system data were sourced from the National Catalogue Service for Geographic Information (Table 1). Additionally, the soil type data were based on 1995 data, and ecological protection area data stemmed from 2018 records. To ensure uniformity, all raster data were resampled to a 500 m resolution before integration into the PLUS model.

Table 1. Data sources.

Data	Sub-Data	Year	Spatial Resolution	Source of Data
Remote sensing image dataset	Remote sensing image	2000 2010 2020	30 m	https://www.gscloud.cn/
Land dataset	Land use	2000 2010 2020	30 m	https://www.resdc.cn/
Socio-economic dataset	Population	2020	1 km	https://www.resdc.cn/
	GDP	2020	1 km	https://www.resdc.cn/
	Primary roads	2021	Vector data	https://www.webmap.cn/
	Secondary roads	2021	Vector data	https://www.webmap.cn/
	Tertiary roads	2021	Vector data	https://www.webmap.cn/
	Seat of county government	2021	Vector data	https://www.webmap.cn/
Natural condition dataset	Temperature	2020	1 km	https://www.resdc.cn/
	Precipitation	2020	1 km	https://www.resdc.cn/
	Elevation	2020	30 m	https://www.gscloud.cn/
	Slope	2020	30 m	https://www.gscloud.cn/
	Soil types	1995	1 km	https://www.resdc.cn/
Constrained dataset	Ecological protection area	2018	Vector data	https://www.resdc.cn/
	River system	2021	Vector data	https://www.webmap.cn/

Note: The access date for the same URL is consistent with the one mentioned above.

2.3. Methodology

2.3.1. The Classification of the PELS

This study draws on the research results of existing classification systems for the PELS [29], categorizing land use data into production space, ecological space, and living space based on different human needs. The PELS can be defined as follows. Production space: a space dominated by production functions, mainly providing human beings with biomass products, non-biomass products, and related services. Ecological space: a space dominated by ecological functions, providing ecological products and services, primarily responsible for the formation and maintenance of ecological systems and processes, natural conditions for human survival, and their utility space. Living space: a space dominated by living functions, where humans engage in various activities to meet various needs such as living, entertainment, healthcare, and education. This classification includes 3 primary categories and 8 secondary categories [30], which are used to identify and classify the PELS in the HCUA (Table 2).

Table 2. PELS classification system in HCUA.

Primary Classification	Second Classification	Secondary Classification of Land Use
Production space (P)	Agricultural production space (P1)	Paddy field and dryland
	Industrial and mining production space (P2)	Other construction land
Ecological space (E)	Forestry ecological space (E1)	Woodland, shrubland, dredged woodland, other woodland
	Grassland ecological space (E2)	High-cover grassland, medium-cover grassland, low-cover grassland
	Water ecological space (E3)	Canals, lakes, reservoirs, permanent glaciers and snow, tidal flats
	Other ecological space (E4)	Sandy land, saline–alkali land, marshland, bare land, bare rock stony land
Living space (L)	Urban living space (L1)	Urban land
	Rural living space (L2)	Rural residential areas

2.3.2. PLUS Model

1. Core Algorithm of PLUS Model

The PLUS model, developed in C++ by the High-Performance Spatial Computational Intelligence Laboratory at China University of Geosciences (Wuhan), serves as a pivotal land use change simulation model [51]. This model integrates a rule-mining framework grounded in the Land Expansion Analysis Strategy (LEAS) along with a Cellular Automaton (CA) model based on Multi-Type Random Patch Seeds (CARS). It facilitates the exploration of the underlying factors driving land expansion and landscape alterations and has found extensive applications in land use simulation research [51,52].

The model's construction logic is as follows: The Land Expansion Analysis Strategy extracts the expansion of each land use type between distinct timeframes. It then employs the Random Forest algorithm to analyze the determinants of expansion for each land use category, discerning the development probability and the impact of various factors on expansion over that period. Concurrently, the CA model, utilizing the Multi-Type Random Patch Seeds method, dynamically adjusts through iterative processes based on the gap between the anticipated demand for land types and the existing stocks of each type, ensuring alignment with the anticipated quantification of land types [53].

The PLUS model can dynamically simulate patch-level changes in multiple land use types, allowing it to be used to study landscape dynamics in the HCUA. It compensates for the shortcomings of existing CA models, such as CA–Markov, CLUE-S, and FLUS, in terms of transformation rule-mining strategies and landscape dynamic change simulation strategies. Some studies have confirmed that [54], compared to the FLUS and CA–Markov models, the PLUS model achieves higher simulation accuracy and more similar landscapes [55].

2. Scenario setting

The multi-scenario design aims to simulate the trends in land use changes under different future development scenarios to analyze the spatial–temporal evolution of land use and land use conflicts in the HCUA. Based on the requirements of the "Harbin–Changchun Urban Agglomeration Development Plan", the "Outline of the 14th Five-Year Plan and 2035 Visionary Goals for National Economic and Social Development of Heilongjiang Province", and the "Outline of the 14th Five-Year Plan and 2035 Visionary Goals for National Economic and Social Development of Jilin Province", this study simulates the land use patterns of the HCUA by setting up a natural development scenario and an

economic development scenario. At the same time, drawing from previous research findings [31,32,53,56,57], this study also sets up a cultivated land protection scenario and an sustainable development goals scenario in the context of the "Three Red Lines" and "Sustainable Development Goals".

The scenarios are described as follows:

(1) Natural Development (ND) Scenario: This scenario represents a continuation of the land use change trends observed from 2010 to 2020, without modifications to diverse parameters or the incorporation of any policy restrictions affecting land use alterations. Under this scenario, the land use demand for the year 2030 is forecasted utilizing the Markov Chain embedded in the PLUS model, with 10-year intervals. The model parameters, including land use expansion capacity, land use transfer matrix, field factor weights, and the transfer probabilities of land use types, are kept constant in alignment with the model spanning from 2010 to 2020.

(2) Cultivated Land Protection (CP) Scenario: This scenario emphasizes the safeguarding of stable and high-quality cultivated land within the HCUA. By overlaying the cultivated land data from the years 2000, 2010, and 2020, regions cultivated consistently across all three time periods are recognized as long-term stable cultivated land in the region [55]. Additionally, based on the "Agricultural Land Grading Procedure" and previous studies [55,58], cultivated land with a slope of less than 6° is extracted as high-quality cultivated land. Stable and high-quality cultivated lands are combined and treated as restricted conversion areas. Moreover, based on the ND and relevant research [8], the land use transfer matrix and transfer probabilities are adjusted to limit other land types from occupying cultivated land. The probability of transferring E1, E2, and E4 to P1 is increased, ensuring the protection of high-quality cultivated land and strict implementation of cultivated land protection policies.

(3) Economic Development (ED) Scenario: Based on previous research results [59], the HCUA is still under pressure from rapid urbanization. In recent years, China has been deeply implementing the overall regional development strategy, with a focus on the *Belt and Road* initiative and the comprehensive revitalization of the northeast, bringing new opportunities for economic development. According to the "Harbin–Changchun Urban Agglomeration Development Plan", the region will continue to expand its openness, strengthen the Harbin–Daqing–Qiqihar–Mudanjiang development belt and the Changchun–Jilin–Tumen development belt, and focus on building the China–Mongolia–Russia Economic Corridor and the Tumen River area as a development and opening-up pioneer zone. In this scenario, no restricted conversion areas are set, and the probability of converting P1, E1, E2, and E4 to P2, L1, and L2 is increased. The occupation of P2, L1, and L2 by other land types is restricted.

(4) Sustainable Development Goals (SDGs) Scenario: The "2030 Agenda for Sustainable Development" adopted by all United Nations member states in 2015 provides a shared blueprint for peace and prosperity for people and the planet, both now and in the future [60]. Its core consists of 17 SDGs, which urgently require action by all countries—developed and developing—in a global partnership to achieve progress in production space, living space, and ecological space, thereby realizing the vision of sustainable development. Under this scenario, ecological protection areas and water source protection zones within the HCUA are treated as restricted conversion areas. Based on the CP and ED scenarios, the probability of converting production and living spaces to ecological space is appropriately increased, aiming to achieve the sustainable development goals.

The classification of different land use transfer matrices for the four scenarios is shown in Table 3 [55]. In the transition matrix, 0 indicates that conversion is not allowed, and 1 indicates that conversion is allowed.

Table 3. Transition matrix under four scenarios.

—	Scenario A (ND)								Scenario B (CP)								Scenario C (ED)								Scenario D (SDGs)							
	a	**b**	**c**	**d**	**e**	**f**	**g**	**h**	**a**	**b**	**c**	**d**	**e**	**f**	**g**	**h**	**a**	**b**	**c**	**d**	**e**	**f**	**g**	**h**	**a**	**b**	**c**	**d**	**e**	**f**	**g**	**h**
a	1	1	1	1	1	1	1	1	1	0	0	0	0	0	0	0	1	1	1	1	1	0	1	1	1	1	1	1	0	0	1	1
b	1	1	1	1	1	1	1	1	1	1	1	1	1	1	1	1	0	1	0	0	0	0	0	1	1	1	1	1	1	1	1	1
c	1	1	1	1	1	1	1	1	1	1	1	1	1	1	1	1	1	1	1	1	1	1	1	1	1	1	1	1	0	1	1	1
d	1	1	1	1	1	1	1	1	1	1	1	1	1	1	1	1	1	1	1	1	1	1	1	1	1	1	1	1	1	1	1	1
e	0	0	0	0	1	0	0	0	1	0	0	0	1	0	0	0	1	1	1	1	1	1	1	1	1	1	0	1	1	1	1	1
f	1	1	1	1	1	1	1	1	1	1	1	1	1	1	1	1	1	1	1	1	1	1	1	1	1	1	1	1	1	1	1	1
g	1	1	1	1	1	1	1	1	1	1	0	1	0	0	1	1	0	0	0	0	0	0	1	0	0	0	0	1	1	0	1	0
h	1	1	1	1	1	1	1	1	1	1	1	1	1	0	1	1	0	0	0	0	0	0	1	1	1	1	1	1	1	0	1	1

Note: a, b, c, d, e, f, g, and h represent P1, P2, E1, E2, E3, E4, L1, and L2, respectively.

3. Determination of neighborhood weight parameters

The neighborhood weight (NW) is used to represent the strength of the ability of various land use categories to expand or transform into other land use categories [61]. Some scholars believe that the total area (TA) change in each land type over the same time scale better reflects its expansion intensity [62]. The dimensionless value of TA change meets the parameter requirements of neighborhood weights in the model in terms of both data meaning and data structure [8]. Therefore, in this study, the calculation formula for neighborhood weight in the PLUS model is as follows:

$$NW_i = \frac{TA_i - TA_{min}}{TA_{max} - TA_{min}} \quad (1)$$

where NW_i represents the neighborhood weight of the i-th land type; TA_i represents the expansion area of the i-th land use type; TA_{min} represents the minimum expansion area of each land use type; TA_{max} represents the maximum expansion area of each land use type. According to the amount of TA change in land types in the HCUA from 2010 to 2020, we calculated their neighborhood weights, as shown in Table 4, and we used the data in the table as the parameters of the neighborhood weights in the PLUS model.

Table 4. Weight of each variety according to TA.

Variety	a	b	c	d	e	f	g	h
TA	3754	985	−2713	−6860	−6145	9350	1780	−151
Weight	0.65	0.48	0.26	0 *	0.04	1 *	0.53	0.41

Note: * According to the actual land expansion situation, the land use type with a weight of 0 is artificially set to 0.1, and the land use type with a weight of 1 is artificially set to 9.9. a, b, c, d, e, f, g, and h represent P1, P2, E1, E2, E3, E4, L1, and L2, respectively.

2.3.3. Spatial Comprehensive Conflict Index (SCCI)

The landscape is the direct object of human resource development and utilization, making it an appropriate scale for studying the impact of human activities on the environment [63]. Landscape ecological risk is considered an effective indicator of absolute land use conflict [17].

Land use conflict is closely related to landscape ecological risk, and the evaluation dimensions of both can correspond to each other. Absolute conflict aims to assess the capacity of land resources to withstand conflict pressures, indicating the stability of the land system, which can be reflected by the level of regional ecological security risk [8]. Therefore, based on existing research, this study adopts the landscape ecological index as an indicator of absolute conflict. We consider the complexity, fragility, and stability of the

land system to construct the SCCI to measure the PELS absolute conflict. The formulas are as follows:

1. Spatial comprehensive conflict index (SCCI)

$$\mathrm{SCCI} = \mathrm{CI} + \mathrm{FI} + \mathrm{SI} \tag{2}$$

where CI represents the complexity index of the space, FI represents the fragility index of the space, and SI represents the stability index of the space. The final calculated results should be calibrated to the (0, 1) range according to Formula (6).

2. Complex index (CI)

$$\mathrm{CI} = \mathrm{AWMPFD} = \sum_{i=1}^{n}\sum_{j=1}^{n}\left[\frac{2\ln(0.25P_{ij})}{\ln a_{ij}}\frac{a_{ij}}{A}\right] \tag{3}$$

where P_{ij} is the perimeter of patch j in spatial type i, a_{ij} is the area of patch j in spatial type i, and A is the total area of the landscape. In fact, this is the formula for the AWMPFD (area-weighted mean patch fractal dimension). The index has proven to be effective in describing the complexity of landscape patterns under human disturbances. A larger value often indicates more complex landscape patterns and more intense land use conflicts caused by human activities.

3. Fragility index (FI)

$$\mathrm{FI} = \sum_{i=1}^{n} F_i \times \frac{a_i}{A} \tag{4}$$

where F_i is the vulnerability of spatial type i, a_i is the area of spatial type i, and A is the total area of the landscape.

Fragility reflects the spatial exposure of landscape types. The fragility of land systems is significantly related to PELS conflicts [64]. The fragility of a particular land use type indicates its degree of response to internal and external pressures, which is the result of PELS conflicts. Therefore, the higher the fragility, the higher the degree of PELS conflicts. Due to the differences in fragility among various spatial types, based on the characteristics of land use changes and the current development status of the HCUA, and drawing from related studies that assign fragility values to different landscape types [65], the fragility indices of P2, L1, L2, E3, E4, P1, E2, and E1 are determined as 6, 6, 6, 5, 4, 3, 2, and 1, respectively. The fragility indices have a maximum value of 6 and a minimum value of 1. These indices are categorized from high to low as extremely fragile, highly fragile, moderately high fragile, moderately fragile, moderately low fragile, and low fragile, in six levels.

4. Stability index (SI)

$$\mathrm{SI} = 1 - \mathrm{PD} = 1 - \frac{M_i}{A} \tag{5}$$

where M_i is the number of patches in a landscape unit i, and A is the area of a landscape unit.

The fragmentation of regional landscapes is a common indication of PELS conflicts. Higher levels of spatial pattern fragmentation correspond to decreased landscape stability and increased conflict intensity [66]. This is because fragmented landscapes indicate high competition between different land use stakeholders [17]. Patch density (PD) serves as a negative indicator reflecting the stability index (SI) of the regional ecosystem. A larger PD value signifies greater spatial fragmentation in the land system and lower stability.

In order to continue the measurement of the SCCI, the linear value in Formulas (2)–(5) is standardized to the range of (0, 1) using the prescribed Formula (6):

$$N = \frac{N_0 - N_{min}}{N_{max} - N_{min}} \quad (6)$$

where N is the value after normalization; N_0 is the value in the common Formulas (3)–(5); N_{min} is the minimum value; N_{max} is the maximum value.

Previous research has indicated that the cell size for the moving window method can be effectively determined using the semi-variogram function [8,31]. Firstly, window cell grids were set at intervals of 10,000, 15,000, 20,000, and 25,000 m, and spatial distribution grid maps for each landscape index were generated. Next, we simulated the semi-variogram models of the landscape indices at different moving window sizes and calculated the ratio ($C_0/(C + C_0)$) of Nugget (C_0) and Sill ($C + C_0$) for three models. According to previous studies [67], $C_0/(C + C_0) < 25\%$ indicates autocorrelation, $25\% \leq C_0/(C + C_0) \leq 75\%$ indicates a moderate correlation, and $C_0/(C + C_0) > 75\%$ indicates a weak correlation. Therefore, as shown in Table 5, 10,000 m is the optimal moving window size, so the window cell size in this study was set to 10,000 m.

Table 5. Semi-variogram model under different moving window sizes.

-	Gaussian Model			Exponential Model			Spherical Model		
Scale	**N**	**S**	**N/S**	**N**	**S**	**N/S**	**N**	**S**	**N/S**
10,000	0.001	0.005	0.260	0.001	0.008	0.089	0.001	0.005	0.163
15,000	0.012	0.031	0.368	0.007	0.042	0.172	0.009	0.033	0.265
20,000	0.011	0.033	0.338	0.007	0.049	0.141	0.008	0.036	0.230
25,000	0.010	0.029	0.349	0.006	0.038	0.159	0.007	0.030	0.250

Note: N and S represent Nugget and Sill, respectively.

2.3.4. Remote Sensing Ecological Index (RSEI)

Ecological environment quality assessment is an effective method for measuring changes in the ecological environment quality of a region. The RSEI proposed by Hanqiu Xu [68], based on four natural indicators (NDVI, Wet, LST, NDBSI), has been widely recognized and applied by scholars both domestically and internationally for regional ecological environment quality assessment. Its remote sensing definition is as follows:

$$RSEI = f(NDVI, Wet, LST, NDBSI) \quad (7)$$

where NDVI represents the Normalized Difference Vegetation Index, Wet represents the Wetness component, LST represents the Land Surface Temperature, and NDBSI represents the Normalized Difference Built-up and Soil Index.

1. Normalized Vegetation Index (NDVI)

$$NDVI = \frac{\rho_{nir} - \rho_{red}}{\rho_{nir} + \rho_{red}} \quad (8)$$

where ρ_{red} and ρ_{nir} are the red band and near-infrared band, respectively.

2. Wetness component (Wet)

$$Wet = K_1\rho_{blue} + K_2\ \rho_{green} + K_3\rho_{red} + K_4\rho_{nir} + K_5\ \rho_{swir1} + K_6\ \rho_{swir2} \quad (9)$$

where K_1, K_2, K_3, K_4, K_5, and K_6 are constants, and ρ_{blue}, ρ_{green}, ρ_{red}, ρ_{nir}, ρ_{swir1}, and ρ_{swir2} are the blue band, green band, red band, near-infrared band, mid-infrared band 1, and mid-infrared band 2, respectively.

3. Land Surface Temperature (LST)

$$LST = \frac{K_2}{\ln\left[\frac{K_1}{B(T_s)} + 1\right]} \tag{10}$$

where K_1 and K_2 are constants; their values can be found in the remote sensing data header file.

$$B(T_s) = \frac{\left[L_\lambda - L_\uparrow - \tau(1-\varepsilon)L_\downarrow\right]}{\tau\varepsilon} \tag{11}$$

where L_λ is the radiant brightness value in the thermal infrared band, τ is the atmospheric transmittance in the thermal infrared band, and ε is the surface specific emissivity; the values of $L_\uparrow$, $L_\downarrow$, and τ can be found on the NASA website.

$$L_\lambda = gain \times DN + bias \tag{12}$$

where DN is the gray value of the pixel, and gain and bias represent the gain value and bias value of the thermal infrared band, respectively.

4. Normalized Difference Built-up and Soil Index (NDBSI)

$$NDBSI = \frac{IBI + SI}{2} \tag{13}$$

$$IBI = \frac{2\rho_{swir1} / \left(\rho_{swir1} + \rho_{nir} - \left[\frac{\rho_{nir}}{\rho_{nir}+\rho_{red}} + \frac{\rho_{green}}{\rho_{green}+\rho_{swir1}}\right]\right.}{2\rho_{swir1} / \left(\rho_{swir1} + \rho_{nir} + \left[\frac{\rho_{nir}}{\rho_{nir}+\rho_{red}} + \frac{\rho_{green}}{\rho_{green}+\rho_{swir1}}\right]\right.} \tag{14}$$

$$SI = \frac{[(\rho_{swir1} + \rho_{red}) - (\rho_{nir} + \rho_{blue})]}{[(\rho_{swir1} + \rho_{red}) + (\rho_{nir} + \rho_{blue})} \tag{15}$$

where ρ_{blue}, ρ_{green}, ρ_{red}, ρ_{nir}, and ρ_{swir1} are the blue band, green band, red band, near-infrared band, and mid-infrared band 1, respectively.

2.3.5. Relative Conflict Measurement Based on Remote Sensing Index

PELS conflicts are subjective measures of the outcomes of land use changes made by humans, while socio-economic–ecological effects are the objective results of these changes. Changes in land use types can either optimize the land use structure, alleviate human–land conflicts, and improve the ecological environment or exacerbate human–land contradictions. The emergence of land use conflicts inevitably comes with a series of negative effects, such as imbalanced socio-economic development, resource allocation discrepancies, and disruptions to ecological systems. This study constructs a land use conflict model for the PELS in the research area by integrating the comprehensive conflict index and the remote sensing ecological index. The comprehensive conflict index signifies absolute conflict, whereas the remote sensing ecological index denotes relative conflict [43].

$$LURC = [(CRI_{t2} - CRI_{t1}) > 0] \wedge [(RSEI_{t2} - RSEI_{t1}) < 0] \tag{16}$$

$$LURCI = |CRI_{t2} - CRI_{t1}| + |RSEI_{t2} - RSEI_{t1}| \tag{17}$$

where LURC represents the PELS relative conflict area; LURCI is the PELS relative conflict index; CRI is the conflict risk index, which also represents the PELS absolute conflict index

(SCCI); RSEI is the remote sensing ecological index; and t1 and t2 represent the start and end times of a certain period.

2.3.6. Center of Gravity Transfer Model

The center of gravity migration model can objectively describe the characteristics, migration distance, and direction of different land use types during the transfer process within a specific period [30]. The formula is as follows:

$$X_t = \sum_{i=1}^{n}(S_{ti} \times X_i) / \sum_{i=1}^{n} S_{ti} \quad (18)$$

$$Y_t = \sum_{i=1}^{n}(S_{ti} \times Y_i) / \sum_{i=1}^{n} S_{ti} \quad (19)$$

where X_t and Y_t represent the longitude and latitude coordinates of the migration center of each spatial type, S_{ti} is the spatial area of unit i during period t, X_i and Y_i are the longitude and latitude coordinates of the geometric center of unit i, the projection coordinate system is Krasovsky_1940_Albers, and n is the number of units in the study area.

3. Results

3.1. An Analysis of the Evolutionary Characteristics of the PELS from 2000 to 2020

3.1.1. The Spatiotemporal Evolutionary Characteristics of the PELS

This study employed ArcGIS 10.8 software to extract and statistically analyze the spatiotemporal characteristics of the PELS in the HCUA from 2000 to 2020. Throughout the study period, the predominant land use types in the HCUA were P1 and E1, collectively representing over 82% of the total area. However, the proportion of E1 exhibited a decreasing trend, declining from 35.92% in 2000 to 35.58% in 2020. Additionally, the overall trend in the study area indicated a rise in production and living spaces alongside a reduction in ecological spaces (Figure 3).

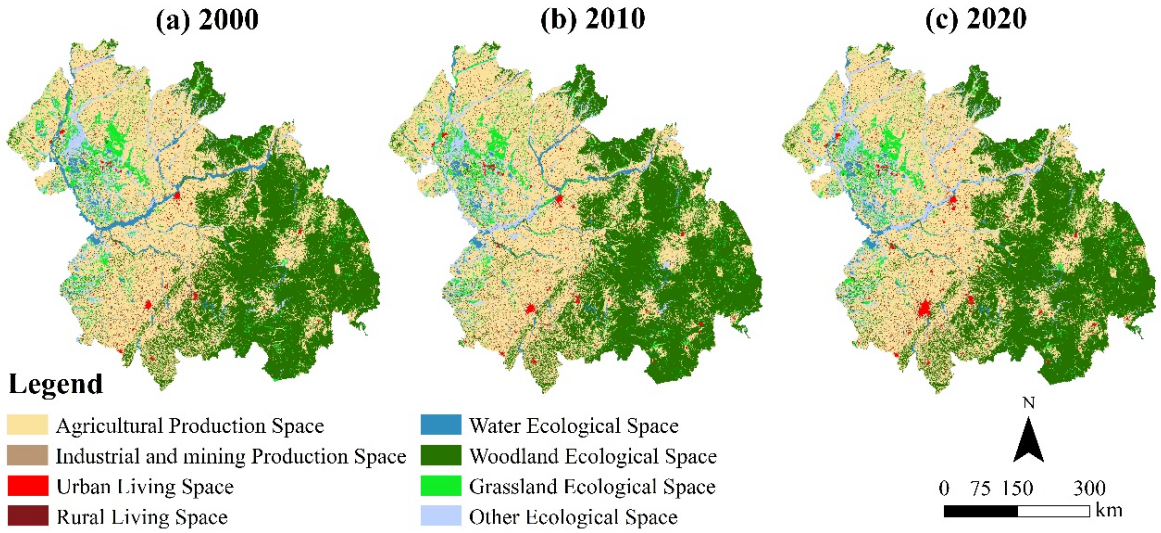


Figure 3. Spatial distribution of PELS from 2000 to 2020.

The spatial distribution of the PELS in the study area remained relatively stable between 2000 and 2020, with no significant changes in the overall structure. However, each type of space exhibited distinct spatial characteristics. E1 was primarily distributed in Yanbian Korean Autonomous Prefecture, Mudanjiang City, Jilin City, Liaoyuan City, eastern Harbin City, and northern Suihua City, displaying a clustering pattern. P1 was

mainly located in Changchun City, Songyuan City, Siping City, Suihua City, Qiqihar City, and western Harbin, primarily associated with the Songnen Plain and Sanjiang Plain. L1 was concentrated along the development belts of Harbin–Daqing–Qiqihar–Mudanjiang and Changchun–Jilin–Tumen, with Harbin and Changchun serving as key development axes. In contrast, L2 had a more dispersed distribution, surrounding L1 evenly. E2 was primarily situated in Daqing City and western Suihua City, with scattered distributions in other cities. E3 was mainly located at the confluence of the Nen River, Songhua River, and Ussuri River. E4 was primarily distributed in Qiqihar City and Daqing City, mainly due to the transition from E3. P2 occupied the smallest area, scattered around the periphery of L1.

In terms of quantity, P1 maintained the dominant position, representing 46.58% in 2000, slightly decreasing to 46.47% in 2010, and then rising to 46.78% in 2020, reflecting an overall trend of an initial decrease followed by an increase. Following P1, E1 accounted for 35.92% in 2000, decreasing to 35.58% by 2020, indicating a continuous decreasing trend. E2 accounted for 5.24% in 2000, decreasing to 5.06% in 2020, showing a trend of a slight initial increase followed by a significant decrease. The proportion of E4 steadily increased from 5.14% in 2000 to 6.20% in 2020. E3 accounted for 3.62% in 2000 and demonstrated a consistent decreasing trend over the study period. Meanwhile, L1, L2, and P2 had smaller proportions at 0.53%, 2.94%, and 0.03% in 2000, respectively, all experiencing notable rapid growth overall (Table 6).

Table 6. The proportion and change in the area of the PELS from 2000 to 2020.

Year/Period	Production Space (%)		Ecological Space (%)				Living Space (%)	
	P1	P2	E1	E2	E3	E4	L1	L2
2000	46.58	0.03	35.92	5.24	3.62	5.14	0.53	2.94
2010	46.47	0.11	35.81	5.59	2.89	5.48	0.70	2.95
2020	46.78	0.19	35.58	5.06	2.41	6.20	0.84	2.94
2000–2010	−0.11	0.07	−0.10	0.35	−0.73	0.33	0.17	0.01
2010–2020	0.31	0.08	−0.23	−0.53	−0.48	0.73	0.14	−0.01
2000–2020	0.20	0.15	−0.33	−0.17	−1.21	1.06	0.31	0.00

3.1.2. The Transformation Characteristics of the PELS

Based on the conversion results of the PELS obtained using ArcGIS 10.8 (Tables 7 and 8), this study utilized Origin 2021 software to visualize spatial patterns (Figure 4). Over the period from 2000 to 2020, the structural transformation within the HCUA predominantly involved the interplay between ecological space and production space, with subsequent shifts observed between production space and living space. Notably, the transformation area between living space and ecological space was the smallest.

Table 7. Land use transfer matrix of HCUA from 2000 to 2010 (unit: km^2).

2010 \ 2000	P1	P2	E1	E2	E3	E4	L1	L2
P1	-	17.43	6872.15	2957.13	1192.64	2196.83	112.38	2917.97
P2	155.38	-	26.98	12.20	37.00	8.12	7.27	44.77
E1	6758.08	6.12	-	1915.65	305.38	740.69	15.41	162.34
E2	3379.34	7.24	2281.75	-	908.59	1696.33	5.68	121.67
E3	1081.97	0.98	322.88	158.38	-	887.75	7.77	44.15
E4	1552.69	2.76	594.55	2113.31	2368.84	-	4.73	61.50
L1	452.74	15.45	21.39	16.07	20.61	20.17	-	209.78
L2	3235.77	7.44	118.73	87.86	33.12	76.32	45.53	-

Table 8. Land use transfer matrix of HCUA from 2010 to 2020 (unit: km^2).

2020 \ 2010	P1	P2	E1	E2	E3	E4	L1	L2
P1	-	65.61	4672.81	2996.41	719.92	1719.09	171.96	2100.49
P2	258.88	-	34.45	52.21	4.37	42.49	26.36	5.55
E1	4251.52	4.98	-	1261.68	76.77	380.81	11.01	54.00
E2	1985.39	6.85	1191.06	-	154.16	1617.17	10.48	67.34
E3	421.84	32.76	108.42	324.51	-	907.77	10.05	11.34
E4	1983.76	7.30	674.35	1978.86	2355.27	-	17.35	72.30
L1	599.50	20.22	29.71	17.75	12.25	20.03	-	117.57
L2	1961.67	35.29	74.95	103.68	23.02	59.59	120.97	-

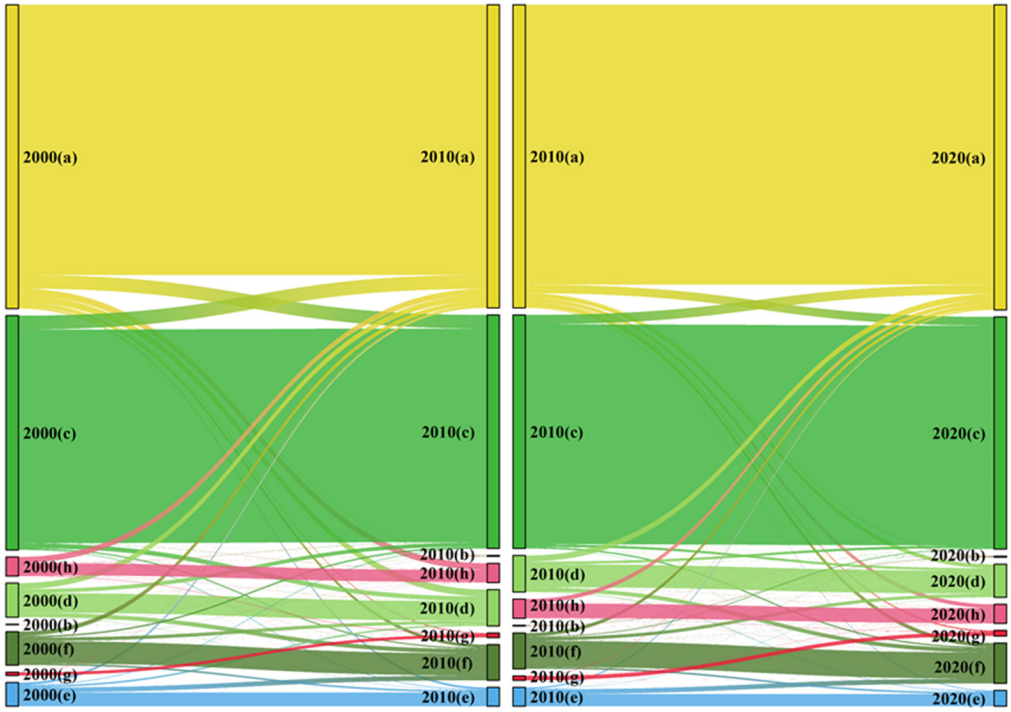


Figure 4. A Sankey diagram of the PELS in the HCUA from 2000 to 2020. Note: a, b, c, d, e, f, g, and h represent P1, P2, E1, E2, E3, E4, L1, and L2, respectively.

During the period spanning 2000 to 2010, P1 experienced significant transformations originating from E1, E2, E4, and L2, with respective conversion rates of 42.25%, 18.18%, 17.94%, and 13.51%. Subsequently, from 2010 to 2020, P1 underwent primary conversions from E1, E2, and L2, capturing rates of 37.54%, 24.07%, and 16.88%, respectively. Across the entire 2000 to 2020 timeframe, P2 predominantly evolved from P1, exhibiting an influx rate of 57.85%. Notably, L1 and L2 during this two-decade period significantly transformed from P1, with influx rates reaching 66.88% and 86.86%, correspondingly. Moreover, the transformations of E1, E2, and E3 were primarily influenced by P1, resulting in a cumulative influx rate of 53.05%. Conversely, E4 predominantly transformed from E3, with an inflow rate of 34.26%.

In terms of outbound transformations, during the period from 2000 to 2010, P1 predominantly transitioned to E1, E2, and L2, with respective exit rates of 40.67%, 20.34%, and 19.47%. From 2010 to 2020, P1 primarily shifted towards E1, E2, E4, and L2, showing exit rates of 37.09%, 17.32%, 17.31%, and 17.11%, respectively. In the same timeframe, P2 mainly transferred to P1 and L1, exiting at rates of 30.36% and 26.90%. Specifically, from 2010 to 2020, P2 predominantly moved towards P1, L1, L2, and E3, with an exit rate of 88.94%. Over the entire duration from 2000 to 2020, L1 and L2 primarily shifted towards

P1, recording an exit rate of 80.86%. E1 primarily transitioned to P1, at a rate of 67.82%. E2 primarily switched to P1 and E4, with exit rates of 42.54% and 29.24%, respectively. E3 mostly changed to E4, with an exit rate of 57.53%. Notably, E4 mainly converted to P1 and E3, exiting at rates of 37.75% and 31.94%.

During the period from 2000 to 2010, the PELS witnessed a total area of mutual transformation amounting to 48,425.74 km^2. This period was characterized by the conversion from ecological space to production space, notably from E1 to P1, predominantly observed in regions rich in lake and river systems, such as the eastern part of Harbin City and the southeastern area of Yanbian Korean Autonomous Prefecture. The transformation was notably influenced by river systems like the Songhua River and Tumen River, enhancing the suitability of the land surrounding water bodies for cultivation. Moving on to the 2010–2020 period, the total area of mutual transformation in the PELS decreased to 36,045.96 km^2 compared to the previous period. This phase mainly involved the mutual transformation between ecological space and production space, with a primary concentration around the Songhua River in Harbin City. Additionally, there was a notable transformation area from production space to living space, focused along the principal development axis of the HCUA, signifying the continual expansion of construction activities encroaching on P1 amidst rapid urbanization.

3.2. The Prediction Results of the PELS Based on the PLUS Model

3.2.1. Accuracy Validation

The validation of accuracy plays a pivotal role in evaluating land use simulation results. This study simulated the spatial distribution of land use in 2020 by leveraging historical trends from 2000 to 2010. A comparison between the simulated 2020 data and actual data was conducted to assess the effectiveness of the PLUS model, as illustrated in Figure 5. The findings revealed that the PLUS model predictions achieved an overall accuracy of 0.88, coupled with a Kappa coefficient of 0.82, surpassing the 0.80 threshold, and the FOM coefficient was 0.357. These results affirm that the PLUS model exhibits a high level of accuracy in simulating land use.

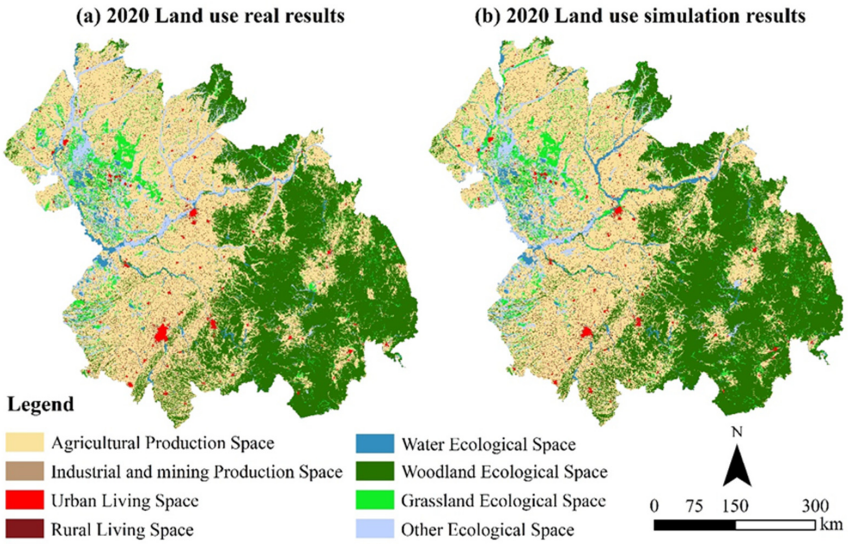


Figure 5. Real and simulated results of PELS maps in 2020.

3.2.2. The Prediction Results of the PELS Under Four Scenarios

This study utilized the PLUS model to simulate the changes in the PELS for four scenarios in 2030 (Figure 6).

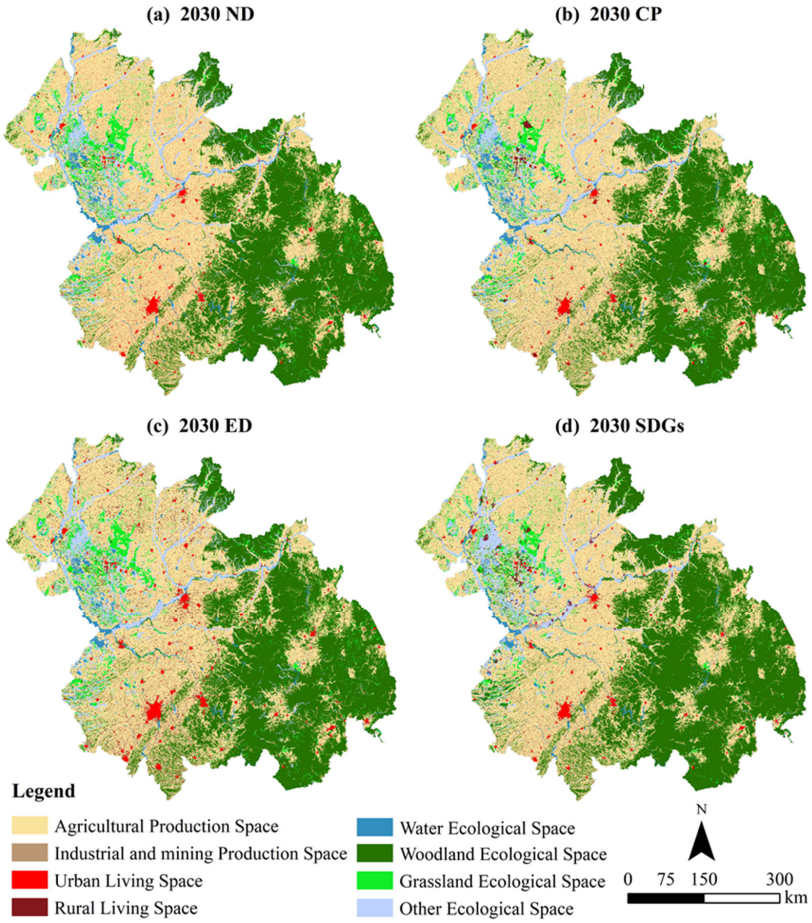


Figure 6. Spatial distribution of PELS under four scenarios. Note: ND, CP, ED, and SDGs represent natural development scenario, cultivated land protection scenario, economic development scenario, and sustainable development goals scenario, respectively.

In the ND scenario, P1 increased from 150,827.19 km^2 in 2020 to 151,487.00 km^2 in 2030, marking a growth of 659.81 km^2, representing a growth rate of 0.44%. L2 also showed growth in 2030 compared to 2020, with an increase of 48.28 km^2, reflecting a growth rate of 0.51%. E3 expanded by 72.59 km^2, reflecting a 0.93% increase. Notably, E4 exhibited the most significant increase, rising from 20,002.52 km^2 in 2020 to 20,821.75 km^2 in 2030, a surge of 819.23 km^2 with a growth rate of 4.10%. Conversely, E2 and E1 experienced the most substantial reductions, declining by 785.20 km^2 and 497.06 km^2, respectively. P2 and L1 also witnessed reductions, with P2 showing the smallest reduction of 36.13 km^2 but the highest decline rate of 6.04%. Spatially, the distribution of different spatial types under this scenario resembled that of 2020, with P1 and E1 each comprising almost half of the HCUA. The primary development axis of Harbin–Changchun acted as a delineation boundary, with P1 dominating the west and E1 the east. L1 exhibited significant clustering in the two provincial capitals, Harbin and Changchun, as well as in other western cities like Qiqihar, Jilin, and Mudanjiang, while L2 was distributed across various regions of the HCUA.

In the CP scenario, the protection of farmland resulted in significant growth, with P1 expanding by 6925.00 km^2 compared to the ND scenario, marking a tenfold increase and a substantial surge in cultivated land area. Both L2 and E3 also experienced growth, with growth rates of 9.67% and 4.82%, respectively. Except for E3, all other ecological spaces witnessed reductions, with E1 notably declining by 4904.56 km^2. E2 showcased the highest reduction rate of 16.46% compared to 2020. Notably, living space demonstrated an upward trend, highlighted by a notable increase in L2, while L1 showed a slight decrease. Spatially, a significant change occurred at the boundary between Daqing City and Suihua

City, where E2 transitioned into L2, yet the overall distribution of the PELS remained largely unchanged.

In the ED scenario, areas designated for economic development, namely L1, L2, and P2, displayed a notable upward trajectory. L1 expanded from 2709.58 km^2 in 2020 to 4221.00 km^2 in 2030, with a substantial increase of 1511.42 km^2 and a growth rate of 55.78%. L2 experienced the most significant growth, escalating from 9468.97 km^2 in 2020 to 13,633.30 km^2, marking a notable rise of 4164.33 km^2 and a growth rate of 43.98%. Although P2 increased by 597.12 km^2, the growth rate notably reached 99.79%. In contrast, P1 decreased by 11,746.00 km^2 compared to the CP scenario and by 4821.00 km^2 compared to the ND scenario. Ecological space, however, exhibited a downward trend, albeit less pronounced than in the CP scenario. Spatially, the cities of Changchun, Harbin, and Jilin saw a clear upward trend in L1 areas.

In the SDGs scenario, there is an amplified emphasis on the harmonized advancement of economic, social, and ecological benefits, alongside the pivotal goals of ensuring food security and attaining sustainable development within the HCUA. Under this scenario, both production space and living space exhibit varying degrees of growth, with growth rates of 15.19% and 21.56%, respectively. Meanwhile, ecological space shows an overall declining trend. Notably, E1 experiences a notable increase compared to the other scenarios, expanding by 5794.50 km^2 compared to the ND scenario. In contrast, E2, E3, and E4 are all decreasing, with E2 experiencing the largest reduction of 4940.45 km^2, representing a decrease rate of 30.27%. Following E2, E3 experiences a reduction of 1874.91 km^2, while E4 experiences the smallest decline at 632.02 km^2. Spatially, the distribution of the PELS under the SDGs scenario aligns with the ND and CP scenarios, with the most notable distinction being the increased presence of L2.

3.3. An Analysis of the Evolutionary Characteristics of the PELS Conflicts from 2000 to 2020

3.3.1. The Spatiotemporal Evolutionary Characteristics of the PELS Absolute Conflicts

This study utilizes the SCCI model and employs Fragstats 4.2 software to calculate landscape pattern indices. A visual analysis of the constructed conflict risk index is conducted to represent the PELS absolute conflict levels in the HCUA for the years 2000, 2010, and 2020. To illustrate the spatial distribution of the PELS absolute conflicts, this paper divides the comprehensive index of spatial conflicts into five levels using equal interval methods based on the distribution characteristics of the cumulative frequency curve of the spatial conflict index and the evolution pattern of the inverted "U" curve model of spatial conflicts [29]: non-conflict [0, 0.2), minor conflict [0.2, 0.4), middle conflict [0.4, 0.6), high conflict [0.6, 0.8), and heavy conflict [0.8, 1.0]. The analysis of the PELS conflict network is performed using ArcGIS 10.8 (Figure 7).

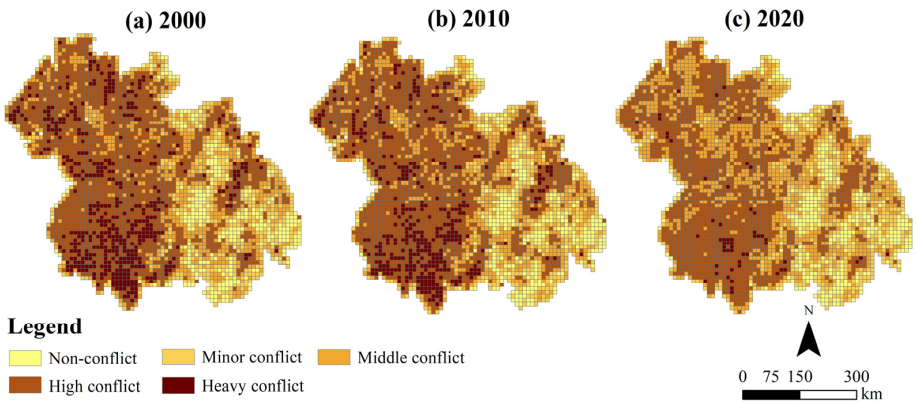


Figure 7. PELS absolute conflicts from 2000 to 2020.

The average comprehensive conflict indices for the HCUA from 2000 to 2020 are 0.5860, 0.5778, and 0.5272, with corresponding standard deviations of 0.2210, 0.2179, and 0.1992. Overall, the PELS absolute conflict risk level shows a decreasing trend over the years. A distinct pattern emerges where the western region exhibits higher conflict levels than the eastern region, and conflicts are more prevalent in plain areas compared to mountainous and hilly regions. As shown in Figure 8, high- and heavy-conflict zones are mainly distributed around the living spaces, notably along the main development axis of Harbin–Changchun and the Harbin–Daqing–Qiqihar–Mudanjiang development belt. Areas classified as non- and minor conflict are primarily located in the eastern part of the HCUA, dominated by E1. In 2000, high-conflict zones accounted for 45.62% of the HCUA area, primarily encircling living spaces, while middle-conflict areas covered 19.57% dispersed across different regions. The heavy-conflict area stood at 47,800 km^2, representing 13.84%, mainly clustered around living spaces due to competition among L1, L2, P1, and E1. The areas of minor and non-conflict accounted for 20.99%, concentrated in the E1 of Mudanjiang City and Yanbian Korean Autonomous Prefecture. By 2010, high conflict continued to dominate, increasing to 46.45%, with an additional 2900 km^2. The proportion of middle-conflict areas increased by 5.33%, remaining relatively dispersed. The area of heavy conflict decreased by 16.53% compared to 2000, while the areas of minor and non-conflict both showed varying degrees of increase, with a total increase rate of 3.47%. By 2020, minor and high conflicts dominated, accounting for a total of 74.47%. The proportion of high-conflict areas decreased by 3.17% and 4.92% compared to 2000 and 2010, respectively. For heavy-conflict zones, there was a significant decline from 47,800 km^2 in 2000 to 5800 km^2 in 2020, reflecting a remarkable decrease rate of 87.87%, constituting only 1.68% of the total HCUA area. Minor and non-conflict areas experienced an increase compared to 2010, registering a total increase rate of 22.75%, nearly 16 times higher than the increase rate observed in 2010.

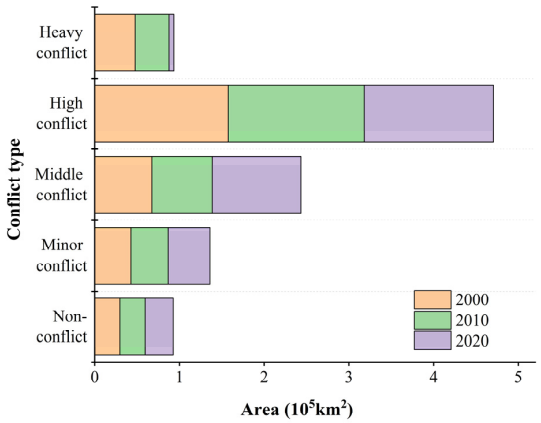


Figure 8. PELS absolute conflict area changes from 2000 to 2020.

To track the spatial evolution trajectory of the PELS absolute conflicts, a center of gravity migration model is used to calculate the migration direction of the PELS absolute conflict center. As shown in Figure 9, from 2000 to 2020, the PELS absolute conflict center migrated southeast, with migration distances of 4558.13 m and 2984.33 m during the periods of 2000–2010 and 2010–2020, respectively. This movement primarily occurred from the peripheral areas of Harbin City to Songyuan City, indicating that the PELS absolute conflict values in the urban fringe areas remained relatively high. Future development must focus on improving the PELS distribution of urban fringe areas and urban–rural junctions to mitigate PELS absolute conflicts in the HCUA. Furthermore, the change in the

elliptical area across the three periods was minimal, indicating a limited coverage range and low dispersion in spatial expansion.

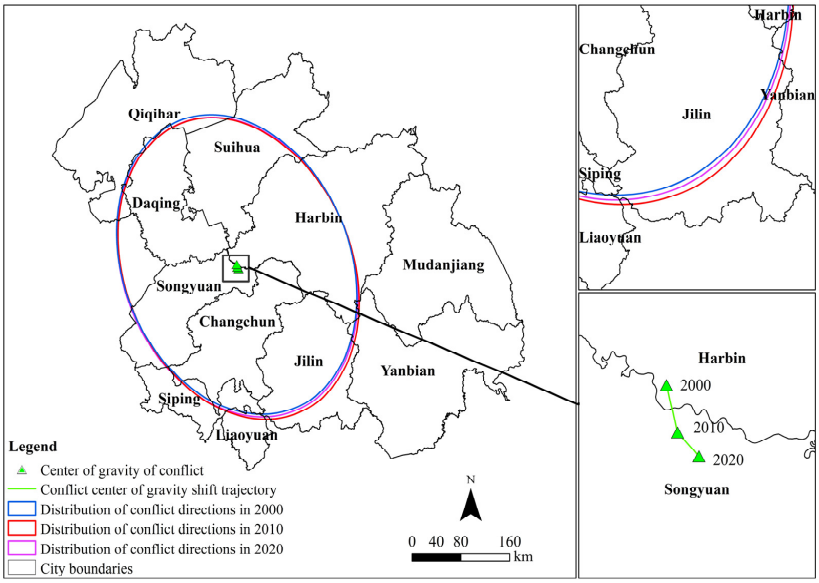


Figure 9. PELS absolute conflict direction migration gravity center from 2000 to 2020.

3.3.2. The Spatiotemporal Evolutionary Characteristics of the PELS Relative Conflicts Evolutionary Characteristics of Ecological Environment Quality

The Google Earth Engine (GEE) platform is utilized to perform principal component analysis on four indicators (NDVI, Wet, LST, NDBSI). This analysis is used to calculate the characteristic values and contribution rates of principal components for the HCUA from 2000 to 2020. The results indicate that the first principal component (PC1) of the RSEI for the years 2000, 2010, and 2020 have characteristic values of 0.0326, 0.0202, and 0.0196, with corresponding contribution rates of 77.20%, 74.84%, and 68.04%, respectively. PC1 has the largest contribution rate, consistently exceeding 68%. This shows that PC1 contains the vast majority of the synthetic information from the remote sensing indices and can be used to calculate the RSEI, thereby reflecting the ecological environment quality status in the study area (Table 9).

Table 9. Principle component (PC) analysis of RSEI indicators of HCUA from 2000 to 2020.

Year	Index	PC1	PC2	PC3	PC4
2000	WET	0.2152	−0.1485	−0.2700	0.9267
	NDVI	0.6223	−0.6102	0.4795	−0.1026
	NDBSI	−0.3639	0.2201	0.8297	0.3615
	LST	−0.6588	−0.7464	−0.0936	0.0061
	Eigenvalue	0.0326	0.0058	0.0029	0.0009
	Eigenvalue contribution rate/%	77.2000	13.6400	6.9600	2.2000
2010	WET	0.2589	−0.1241	−0.4493	0.8460
	NDVI	0.5721	−0.5249	0.6251	0.0800
	NDBSI	−0.4149	0.3862	0.6372	0.5221
	LST	−0.6585	−0.7482	−0.0351	0.0731
	Eigenvalue	0.0202	0.0045	0.0015	0.0008
	Eigenvalue contribution rate/%	74.8400	16.5300	5.5800	3.0500
2020	WET	0.0618	0.0711	0.5157	−0.8516
	NDVI	0.7956	−0.4136	−0.3885	−0.2121
	NDBSI	−0.4634	0.0527	−0.7434	−0.4794
	LST	−0.3853	−0.9061	0.1745	0.0021
	Eigenvalue	0.0196	0.0070	0.0019	0.0002
	Eigenvalue contribution rate/%	68.0400	24.4900	6.7100	0.7600

Analyzing the variations in each indicator, as illustrated in Table 10, reveals notable trends in the mean values. Specifically, the mean values of the NDVI and Wet, indicative of favorable ecosystem conditions, demonstrated an overall upward trajectory over the study period. Conversely, LST and NDBSI, representing poor ecological factors, exhibited a general decline. The NDBSI experienced a 9.07% increase from 2000 to 2010, followed by a notable 48.67% decrease from 2010 to 2020, indicating an overall downward trend. Regarding the LST indicator, there was an initial decrease and subsequent increase from 2000 to 2020, with decline and growth rates of 7.21% and 2.02%, respectively. Collectively, these indicators portray a positive trend in the ecological quality of the research area.

Table 10. Statistics of four indicators and RSEI of HCUA from 2000 to 2020.

Year	Value	WET	NDVI	NDBSI	LST	RSEI
2000	Minimum	−0.8961	−0.3157	−0.4309	7.1311	0.0000
	Maximum	0.4673	0.5590	0.3022	27.8914	1.0000
	Mean	−0.1209	0.2455	−0.0827	21.3125	0.6159
	Std Dev	0.0841	0.1194	0.0621	2.7205	0.1494
2010	Minimum	−1.0398	−0.5737	−0.4342	6.2582	0.0000
	Maximum	0.4509	0.6999	0.5282	26.4335	1.0000
	Mean	−0.0931	0.2393	−0.0752	19.7757	0.6196
	Std Dev	0.0839	0.1268	0.0695	2.1417	0.1208
2020	Minimum	−0.6936	−0.4717	−0.4205	6.2932	0.0000
	Maximum	0.5268	0.5920	0.3855	28.6475	1.0000
	Mean	−0.0453	0.2863	−0.1118	20.1751	0.7025
	Std Dev	0.0490	0.1613	0.0652	2.0872	0.1359

The RSEI is classified into five levels using an equal interval method: $0 \leq \text{RSEI} < 0.2$, $0.2 \leq \text{RSEI} < 0.4$, $0.4 \leq \text{RSEI} < 0.6$, $0.6 \leq \text{RSEI} < 0.8$, and $0.8 \leq \text{RSEI} \leq 1$, corresponding to poor, comparatively poor, intermediate, good, and the best ecological environment quality, respectively. Furthermore, the SCCI and RSEI of the HCUA from 2000 to 2020 are standardized, with the statistical results presented in Table 11. The average RSEI values for the years 2000, 2010, and 2020 are 0.6159, 0.6196, and 0.7025, respectively. The increases in RSEI averages from 2000 to 2010 and 2010 to 2020 were 0.60% and 13.38%, indicating a rapid overall improvement in the ecological environment quality of the HCUA from 2000 to 2020. Meanwhile, the average and standard deviation of the SCCI showed a gradual downward trend over time, indicating a yearly decrease in absolute conflict values and an annual improvement in ecological environment quality.

Table 11. SCCI and RSEI of HCUA from 2000 to 2020.

Year	SCCI		RSEI	
	Mean	Std Dev	Mean	Std Dev
2000	0.5860	0.2210	0.6159	0.1494
2010	0.5778	0.2179	0.6196	0.1208
2020	0.5272	0.1992	0.7025	0.1359

In summary, the calculated RSEI concurs with the outcomes delineated by the four indicators and effectively encapsulates their essence. Merely considering individual indicators might neglect their interactions, impeding a holistic assessment across various metrics. The adoption of the integrated RSEI not only amalgamates the disparate indicators but also offers a thorough evaluation of ecological environment quality within the HCUA, succinctly quantifying the extent of ecological quality variation. Hence, it provides a superior approach compared to single-indicator analyses.

The experimental results derived from the RSEI outline the following key findings: (1) From 2000 to 2020, the ecological environment quality within the HCUA displayed

a consistent annual enhancement trend, with poor and comparatively poor ecological environments primarily located in the western plain areas of the HCUA, while the eastern mountainous areas exhibit better ecological environment quality. (2) Amidst the rapid economic development and revitalization of the old industrial base in Northeast China, the overall ecological environment quality of the HCUA was poor in 2000, especially in cities such as Harbin, Changchun, Songyuan, Suihua, and Qiqihar. These cities neglected ecological considerations while pursuing economic growth, resulting in intense PELS conflicts across the region. (3) Subsequent to the sustained implementation of sustainable development strategies, there was a noticeable upturn in ecological environment quality from 2010 to 2020, especially in the post-implementation of the "Harbin–Changchun Urban Agglomeration Development Plan", which further expanded areas with improved ecological environment quality. By 2020, the ecological environment quality in the HCUA was predominantly rated as good. The specific distribution of the RSEI is shown in Figure 10.

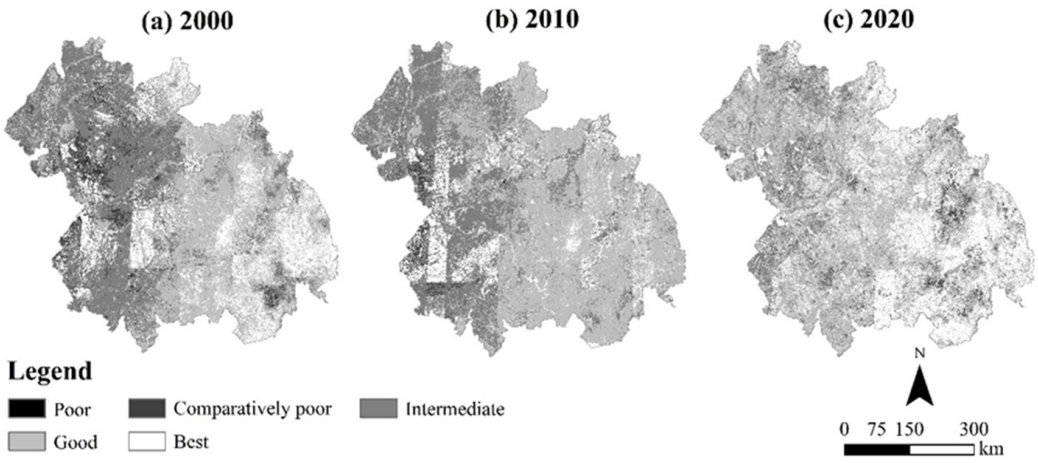


Figure 10. RSEI level of HCUA in 2020.

Spatiotemporal Evolutionary Characteristics of the PELS Relative Conflicts

This study employs Formulas (16) and (17) to obtain normalized PELS relative conflict areas and conflict intensity for two time periods: 2000–2010 and 2010–2020. Using ArcGIS 10.8 software, the spatial patterns of the PELS relative conflicts are visualized (Figure 11). The spatial relative conflict levels are classified into three grades using natural breaks: $0 \leq \text{LURCI} \leq 0.2$ is classified as minor conflict, $0.2 < \text{LURCI} \leq 0.4$ as middle conflict, and $0.4 < \text{LURCI} \leq 1$ as high conflict. The statistical results of the PELS relative conflicts are shown in Table 12: (1) Throughout both 2000–2010 and 2010–2020, minor-conflict regions encompassed more than 50% of the total spatial area, significantly influencing sustainable development efforts and the mitigation of PELS conflicts. (2) The average values of PELS relative conflicts during 2000–2010 and 2010–2020 were 0.21 and 0.23, with corresponding standard deviations of 0.17 and 0.16, indicating an overall upward trend in the PELS relative conflict intensity. (3) The relative conflict areas during 2000–2010 were primarily minor conflicts, but the proportion of minor-conflict areas decreased from 56.17% to 53.04%, a decrease of 5.57%. The areas of middle conflict increased by 10.38%, rising from 29.56% to 32.63%. The areas of high conflict increased by 200 km^2, with a growth rate of 0.41%, and their proportion rose from 14.27% to 14.33%.

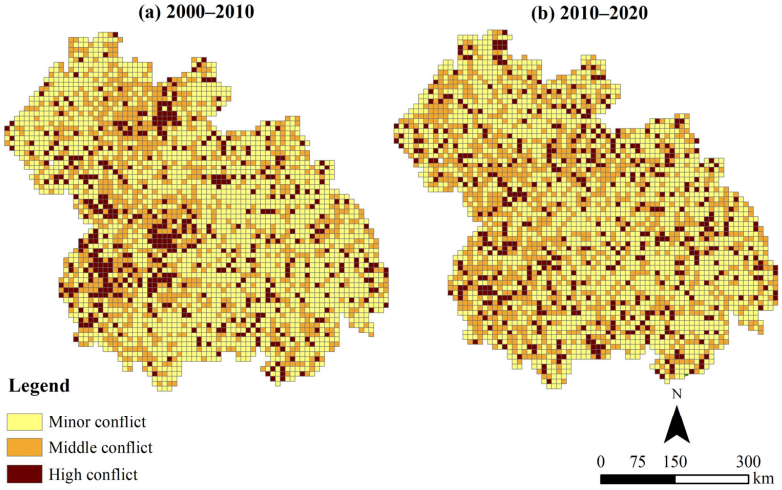


Figure 11. PELS relative conflict levels from 2000 to 2020.

Table 12. Transfer matrix of PELS relative conflicts from 2000 to 2020 (unit: km^2/%).

Conflict Level		2020				
		Minor Conflict	Middle Conflict	High Conflict	Total	Proportion
2000	Minor conflict	126,100	58,300	9600	194,000	56.17
	Middle conflict	45,100	39,000	18,000	102,100	29.56
	High conflict	12,000	15,400	21,900	49,300	14.27
	Total	183,200	112,700	49,500	345,400	100.00
	Proportion	53.04	32.63	14.33	100.00	——

By examining the temporal and spatial evolution patterns of the PELS, it was observed that with the urbanization process in the HUCA, PELS relative conflicts were more prevalent in the western plain areas, which also exhibited the most significant changes in land use cover. This was mainly characterized by living spaces encroaching on production spaces, with farmland being converted to construction land.

From Figure 11, it can be seen that during 2000–2010, minor- and middle-conflict areas were widely distributed with clear spatial differentiation, primarily concentrated in ecological spaces. In contrast, high-conflict areas were more concentrated, mainly located at the boundaries of production and living spaces in cities such as Suihua, Harbin, Changchun, Songyuan, and Daqing. During 2000–2010, high-conflict areas in the HCUA were primarily located in the periphery of L1. This was due to the influence of human factors such as policies, planning, and transportation layout, which made economic development in the peripheral areas less constrained than that in L1, resulting in an increase in conflict risk indices and a decline in the RSEI. From 2010 to 2020, minor conflicts continued to dominate, but the areas of middle and high conflicts increased, indicating an escalation in conflict intensity. The spatial distribution of high-conflict areas became more scattered, appearing in various districts of the HCUA, with middle- and high-conflict areas further expanding outward from the central areas.

3.4. The Prediction Results of PELS Absolute Conflicts Based on the PLUS Model

3.4.1. The Prediction Results of PELS Absolute Conflicts Under Four Scenarios

The simulation of land use scenarios for the HCUA in 2030 using the PLUS model led to the calculation of the spatial distribution of the composite conflict index under various scenarios (Figure 12). The conflict index was categorized into five levels utilizing equal interval methods: non-conflict [0, 0.2), minor conflict [0.2, 0.4), middle conflict [0.4, 0.6), high conflict [0.6, 0.8), and heavy conflict [0.8, 1.0]. The average comprehensive conflict

indices projected for 2030 under the ND, CP, ED, and SDGs scenarios are 0.5281, 0.5318, 0.5246, and 0.5257, coupled with corresponding standard deviations of 0.1996, 0.2011, 0.2004, and 0.2005, respectively. Overall, the spatial distribution pattern of PELS absolute conflicts under the four scenarios in 2030 is largely consistent with that in 2020, showing higher levels of conflict in the west compared to the east and in living spaces compared to ecological spaces, with conflicts in plain areas being more significant than those in mountainous areas. This reflects a certain path dependency in the evolution of PELS conflicts in the region.

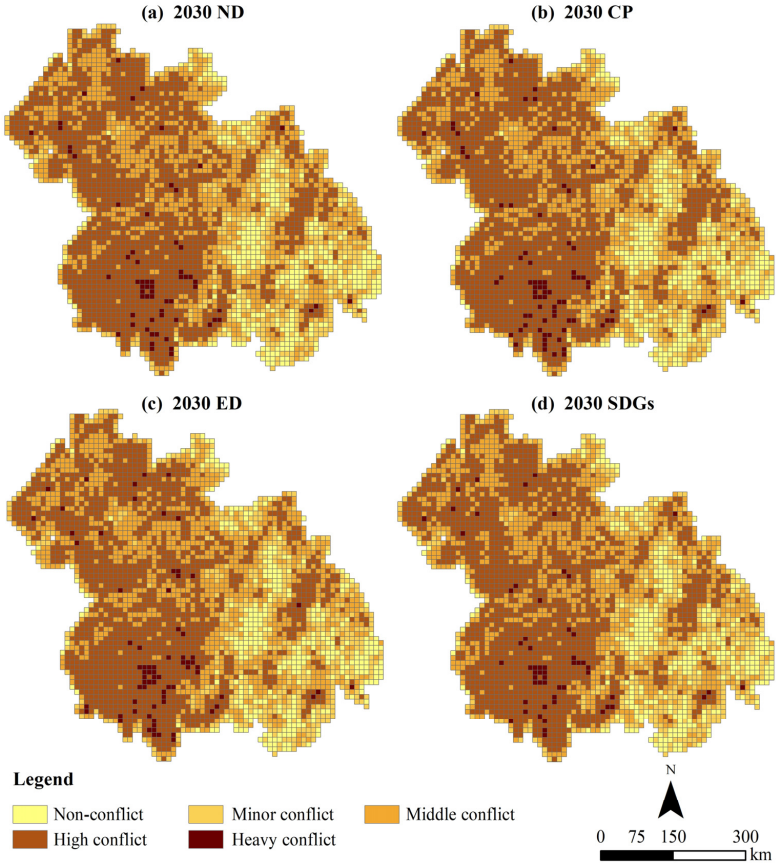


Figure 12. PELS absolute conflicts under four scenarios. Note: ND, CP, ED, and SDGs represent natural development scenario, cultivated land protection scenario, economic development scenario, and sustainable development goals scenario, respectively.

From the differences among scenarios, the ED scenario exhibits the most severe conflict levels. Under this scenario, substantial amounts of P1, E1, E2, E3, and E4 are encroached upon by the expansion of L1, L2, and P2, resulting in a rising trend of conflicts in urban areas. In contrast, the CP and SDGs, due to imposed constraints, maintain a relatively stable land use structure, resulting in lower ecological risks and less intense conflicts. As shown in Figure 13, the areas of various PELS conflict types under the four scenarios are not significantly different, with high-conflict areas predominating, followed by middle-conflict areas. In all scenarios, heavy-conflict areas account for the smallest proportion, remaining below 2.3%. This indicates that heavy-conflict areas in the HCUA are gradually decreasing, while conflicts below the middle level are shifting towards high-conflict levels, suggesting that more actions need to be taken in the future to mitigate PELS conflicts.

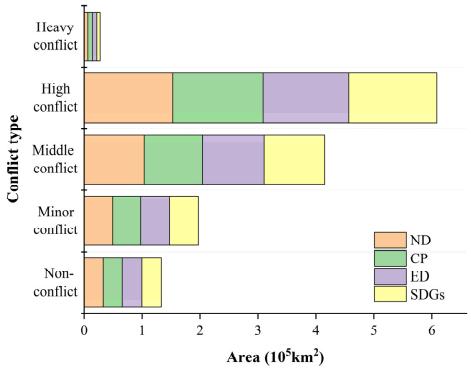


Figure 13. PELS absolute conflict area changes by conflict type under four scenarios. Note: ND, CP, ED, and SDGs represent natural development scenario, cultivated land protection scenario, economic development scenario, and sustainable development goals scenario, respectively.

3.4.2. Change Intensity of PELS Absolute Conflicts Under Four Scenarios

To illustrate the interannual changes in PELS absolute conflicts between 2020 and 2030 under four scenarios, this study visualizes the changes in absolute conflicts using ArcGIS 10.8 (Figure 14). The changes are classified into five levels based on data conditions: SCCIIC < 0 for improvement, SCCIIC = 0 for invariability, 0 < SCCIIC $\leq$ 0.05 for mild deterioration, 0.05 < SCCIIC $\leq$ 0.2 for moderate deterioration, and 0.2 < SCCIIC $\leq$ 1 for severe deterioration, where SCCIIC is the interannual variation in the SCCI. The corresponding statistical results of absolute conflict raster counts are shown in Table 13.

Table 13. The number of grids for interannual changes in absolute conflicts between 2020 and 2030 under four scenarios. Note: A, B, C, and D represent 2020–2030 ND, 2020–2030 CP, 2020–2030 ED, and 2020–2030 SDGs, respectively.

Conflict Degree	A	B	C	D
Improvement	1067	750	556	2204
Invariability	3	3	3	3
Mild deterioration	2382	2656	2764	1175
Moderate deterioration	3	43	131	72
Severe deterioration	0	3	1	1

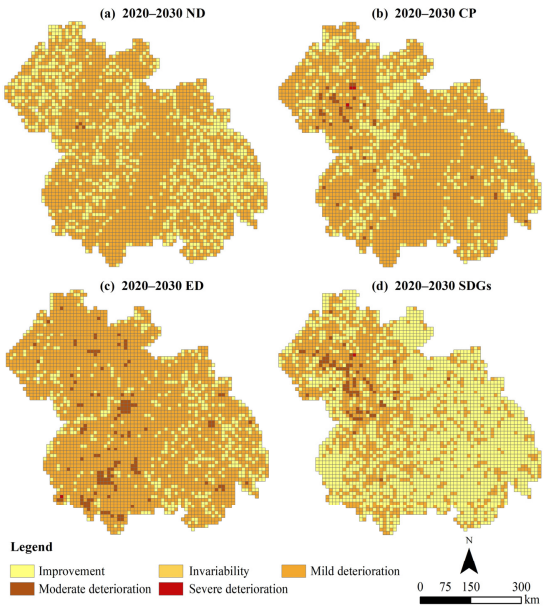


Figure 14. Interannual changes in absolute conflicts between 2020 and 2030 under four scenarios. Note: ND, CP, ED, and SDGs represent natural development scenario, cultivated land protection scenario, economic development scenario, and sustainable development goals scenario, respectively.

From the analysis of Figure 14 and Table 13, the following conclusions can be drawn:

(1) In the 2020–2030 ND scenario, mild deterioration is the predominant change in PELS absolute conflicts, representing 68.94% of the total raster counts. This deterioration is concentrated in Jilin City, Liaoyuan City, Harbin City, Songyuan City, Changchun City, and Suihua City, signifying conflicts between P1 and living spaces. Areas showing improvement account for 30.88%, primarily in E1 and E2. In this scenario, no severe deterioration areas exist, and areas with invariability and moderate deterioration are also minimal.

(2) In the 2020–2030 CP scenario, mild deterioration remains the primary change in absolute conflicts, constituting 76.87% of the total raster counts. The areas of mild deterioration shift towards the southeast and northwest compared to the ND scenario, indicating escalated conflicts between P1 and ecological spaces. The areas showing improvement decreased by 29.71%, primarily in Suihua City and Changchun City. Moderate deterioration areas are concentrated around the urban periphery of Daqing City, reflecting heightened conflicts among ecological, production, and living spaces. Severe deterioration areas are identified between L2 and ecological spaces in Daqing City.

(3) In the 2020–2030 ED scenario, mild deterioration remains the prevalent change, accounting for 80% of the total raster counts across various regions of the HCUA. The number of areas showing improvement decreased to 556, with a dispersed distribution primarily in eastern Mudanjiang City and Yanbian Korean Autonomous Prefecture. Moderate deterioration areas are mainly situated around L1 in Changchun City, Harbin City, and Jilin City, indicating competition between L1 and production spaces.

(4) In the 2020–2030 SDGs scenario, improvements characterize the changes in absolute conflicts, representing 63.79% of the total raster counts mainly distributed in the central and eastern regions. Mild deterioration areas account for 34.01% of the total raster counts, primarily located in Daqing City and Qiqihar City, with scattered occurrences in the central and eastern regions. Moderate deterioration areas, amounting to 2.08%, are mainly found in Daqing City, reflecting conflicts between L2 and ecological spaces. In summary, significant improvements in PELS conflicts within the HCUA are achieved uniquely under this scenario, ensuring progress in the PELS in alignment with the vision of sustainable development.

3.5. Development Strategies of HCUA Based on PELS Conflicts

Based on the analysis of the predicted results for PELS conflicts under different scenarios, the following development strategies are proposed (Figure 15):

1. Urban and Rural Optimization Model

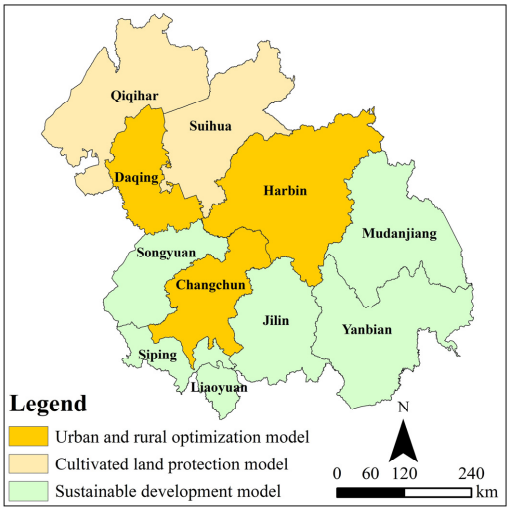


Figure 15. Development strategies for the HCUA.

This model applies to Harbin City, Changchun City, and Daqing City. According to the results regarding the intensity of PELS absolute conflicts, the absolute conflicts in these cities are expected to escalate to varying degrees by 2030 across all scenarios. The main reason for this trend is the accelerated expansion of living spaces encroaching on ecological spaces, specifically characterized by L1 and L2 encroaching on E2 and E4. Additionally, the SCCI forecasts suggest that L1 in Daqing City has a strong radiation effect on the surrounding villages. Therefore, under this model, the structure and layout of L1 and L2 in these cities should be optimized. This includes developing a number of well-established, ecologically livable, small cities; guiding the orderly migration of the rural population to nearby cities; and vigorously promoting urban–rural integration development. Emphasizing the concentrated and efficient development of construction land can effectively reduce spatial fragmentation, thereby forming a more rational population, urban, and economic layout system.

2. Cultivated Land Protection Model

This model applies to Qiqihar City and Suihua City. According to the predicted PELS results in 2030, Qiqihar City and Suihua City will continue to primarily focus on P1. Furthermore, based on the relative conflict results, the relative conflicts in concentrated cultivated land areas eased from 2010 to 2020, which is beneficial for stabilizing food production in the HCUA. However, based on the predicted changes in SCCI intensity under the CP scenario, both Qiqihar City and Suihua City show a predominance of mild deterioration in absolute conflicts, reflecting the contradictions between living spaces and production spaces. Therefore, under this model, Qiqihar City and Suihua City should implement strict cultivated land protection policies to ensure that the area and quality of cultivated land do not decrease. They should also coordinate the structure and layout of living spaces and production spaces; comprehensively enhance agricultural irrigation, mechanization, and informatization levels; and establish a number of core functional areas for food production to secure the region's food supply.

3. Sustainable Development Model

This model is applicable to the central and eastern regions of the HCUA, including Songyuan City, Siping City, Jilin City, Liaoyuan City, Mudanjiang City, and Yanbian Korean Autonomous Prefecture. According to the predicted results of PELS absolute conflicts and their change intensity results, these regions show a significant mitigation of absolute conflicts under the SDGs, primarily indicating positive alterations in conflict dynamics. Therefore, under this model, these cities should maintain the existing ecological protection areas and water source protection ranges while implementing spatial classification control. They should scientifically and reasonably coordinate various land use demands for "production–living–ecology", achieving high efficiency in production spaces, comfortable living spaces, picturesque ecological environments featuring clear mountains, and water bodies, thereby actualizing the vision of sustainable development.

4. Discussion

4.1. Spatiotemporal Evolutionary Characteristics of PELS Absolute Conflicts

From 2000 to 2020, the PELS absolute conflicts in the HCUA displayed a consistent improvement trend, with a spatial distribution pattern characterized by a stronger presence in the west and weaker in the east. Monitoring changes indicate that conflicts within the PELS are more severe in the western areas of the urban agglomeration, whereas those in the eastern regions remain relatively stable. Wei Zhang's research revealed that regions prone to conflict are concentrated in core areas with high economic development and population density, contrasting with the less conflicted nature reserves and key ecological function areas

in the northwest and east [31], which align with the findings of this study. The eastern part of the HCUA primarily consists of mountainous and hilly areas, whereas the western part mainly consists of plains. Severe, high, and moderate conflicts are predominantly found in lower-altitude, relatively flat plain areas, while light and conflict-free areas are primarily distributed in higher-altitude, densely vegetated, and relatively rugged mountainous and hilly regions. Zhaoyang Wang conducted a multi-scale study on land use conflicts in Chongqing City and found that socio-economic activities tend to maximize benefits by utilizing flat, easily developed land. Areas of severe and moderate land use conflicts are consistently concentrated in economically active, lower-altitude, and relatively flat central urban areas and their surrounding regions, while light and general conflict areas are primarily found in higher-altitude, densely vegetated, relatively rugged regions with weak human economic activities [32], which corresponds with the findings of this study. However, Ya Peng's analysis of land use conflicts in Urumqi City identified that despite being classified as zones of medium-high ecosystem service value, areas abundant in mountainous forests are more susceptible to land use conflicts due to natural ecological progression and human intervention [64], differing somewhat from the conclusions of this study.

The multi-scenario simulation results of this study indicate that the spatial pattern of conflicts within the HCUA will largely preserve the status observed in 2020, suggesting a certain continuity in the development and evolution of PELS conflicts. Studies by Meimei Wang, Xiao Zhang, and Bo Wang on land use conflict scenario simulations in the Xining metropolitan area, the Yangtze River Delta urban agglomeration, and Poyang Lake region, respectively [8,56,57], also revealed a level of consistency in future conflict spatial distributions, echoing the findings of this research. However, this study identifies that the HCUA experiences the most intense conflicts under the ED scenario, followed by the CP scenario. In contrast, Bo Wang's research noted that the most intense conflicts in Poyang Lake region occur under the ED scenario for 2035, with the ND scenario ranking next. Xiao Zhang's findings indicated that the most intense conflicts in the Yangtze River Delta urban agglomeration occur under the ND scenario for 2030, followed by the ED scenario. This discrepancy could be attributed to the significant cultivated land area within the HCUA, serving as a crucial "granary" in China, leading to relatively elevated conflict levels under the CP scenario. Nevertheless, the mitigation of conflicts under various scenarios highlights the positive impact of the SDGs in reducing PELS conflicts.

4.2. Spatiotemporal Evolutionary Characteristics of PELS Relative Conflicts

During the study period, the interactions between production, residential, and ecological zones within the HCUA showcased that the prevailing conflicts arising from land utilization predominantly consisted of mild conflicts from 2000 to 2020. Regions experiencing moderate and high conflicts progressively expanded outward from the central core, primarily concentrated in the expanding urban residential zones, demonstrating an overall upward trajectory. Deling Wang's research in Nanchang City on relative conflicts revealed a prevalence of mild-conflict areas during both the 2000–2010 and 2010–2020 periods, with moderate-conflict zones shifting from central urban areas towards the outskirts [43], aligning with the findings of this study. Therefore, mitigating PELS conflicts in the western plain regions of the HCUA and ensuring the harmonized development of the PELS in the eastern mountainous and hilly terrains are pivotal for fostering sustainable development across the entire region.

4.3. The Applicability of the PLUS Model

Compared with previous land use change simulation models, the PLUS model proposes land expansion analysis strategies and a multi-type seed growth mechanism, making the simulation of land use patterns closer to the objective spatial patterns of land use, with the highest prediction accuracy, and being the most suitable for complex land use predictions [51]. The prediction results of the PLUS model in this paper show a Kappa coefficient of 0.82, and many scholars have conducted land use simulation studies using the PLUS model [8,31,32,55,56,69], with simulation accuracies all exceeding 0.8. This indicates that the simulation accuracy of the PLUS model has been verified in a wider range of practices and demonstrates good reliability.

5. Conclusions

This study, based on the PELS theory, analyzes the spatiotemporal evolutionary characteristics of the PELS in the HCUA. Using the PLUS model, the development trends in land use under four scenarios are simulated, and the absolute conflicts and relative conflicts of the PELS are analyzed, leading to the following main conclusions.

From 2000 to 2020, land use types are mainly P1 and E1, accounting for over 82% in total, showing an overall trend of increasing production space and living space while decreasing ecological space. Spatially, there is no significant change in the overall spatial distribution structure of the HCUA. In terms of quantity, the area of P1 is the largest, showing a trend of initially decreasing and then increasing with time. In the CP scenario, the cultivated land area experiences substantial growth. Compared to the ND scenario, the most significant change occurs at the junction of Daqing City and Suihua City, where E2 transitions to L2. In the ED scenario, L1, L2, and P2 expand, with L2 experiencing the largest increase, while P1 and ecological space shrink. In the SDGs scenario, there is expansion in both production and living spaces, accompanied by a decrease in ecological spaces, albeit less pronounced than that in the other scenarios.

From 2000 to 2020, the absolute conflict index showed a continuous decreasing trend over time, mainly manifested by the transformation of heavy-conflict areas into minor- and middle-conflict areas. Spatially, the western region is higher than the eastern region, and the plain areas are higher than the mountainous and hilly areas. Calculations using the GEE platform on the RSEI indicated an increasing trend in ecological quality. The mean values of relative conflicts were 0.21 and 0.23 for the periods 2000–2010 and 2010–2020, respectively, with corresponding standard deviations of 0.17 and 0.16, indicating an overall increase in the intensity of relative conflicts. Both relative and absolute conflicts mostly occurred in the western plain areas, which are also the regions with the most intense changes, mainly characterized by conflicts between living space and production space.

Under the ED scenario, the absolute conflict intensity is the most severe, characterized by a significant encroachment of L1, L2, and P2 onto areas occupied by P1, E1, E2, E3, and E4. In contrast, under the CP and SDGs scenarios, the land use structure is relatively stable, and the conflict intensity is relatively moderate. The difference in the area of land use conflict types is not significant across the four scenarios. In the SDGs scenario, from 2020 to 2030, the absolute conflict changes primarily show improvement, while the other three scenarios mainly indicate mild deterioration. Based on this, we propose development strategies using three models: an urban and rural optimization model, cultivated land protection model, and sustainable development model.

Author Contributions: Conceptualization, X.W. and Y.Z.; methodology, X.W.; validation, X.W., Y.Z., and S.C.; formal analysis, X.W.; writing—original draft preparation, X.W.; writing—review and editing, Y.Z.; visualization, X.W.; supervision, Y.Z.; project administration, Y.Z.; funding acquisition, X.L. All authors have read and agreed to the published version of the manuscript.

Funding: This research was funded by the National Natural Science Foundation of China, grant number 42171328.

Data Availability Statement: The original contributions presented in the study are included in the article, further inquiries can be directed to the corresponding author.

Conflicts of Interest: The authors declare no conflicts of interest.

References

1. Hu, Y.; An, R.; Yang, J. Measurement and Driving Mechanism of Land Use Conflict Based on Landscape Pattern: A Case Study of Wuhan Metropolitan Area. *Res. Soil Water Conserv.* **2024**, *31*, 354–364.
2. Zong, S.; Xu, S.; Jiang, X.; Song, C. Identification and Dynamic Evolution of Land Use Conflict Potentials in China, 2000–2020. *Ecol. Indic.* **2024**, *166*, 112340. [CrossRef]
3. Zou, Y.; Meng, J.; Zhu, L.; Han, Z.; Ma, Y. Characterizing Land Use Transition in China by Accounting for the Conflicts Underlying Land Use Structure and Function. *J. Environ. Manag.* **2024**, *349*, 119311. [CrossRef] [PubMed]
4. Zou, L.; Liu, Y.; Wang, J.; Yang, Y. An Analysis of Land Use Conflict Potentials Based on Ecological-Production-Living Function in the Southeast Coastal Area of China. *Ecol. Indic.* **2021**, *122*, 107297. [CrossRef]
5. Nantel, P.; Bouchard, A.; Brouillet, L.; Hay, S. Selection of Areas for Protecting Rare Plants with Integration of Land Use Conflicts: A Case Study for the West Coast of Newfoundland, Canada. *Biol. Conserv.* **1998**, *84*, 223–234. [CrossRef]
6. Yang, L.; Fang, C.; Chen, W.; Zeng, J. Urban-Rural Land Structural Conflicts in China: A Land Use Transition Perspective. *Habitat Int.* **2023**, *138*, 102877. [CrossRef]
7. Pacheco, F.A.L.; Sanches Fernandes, L.F. Environmental Land Use Conflicts in Catchments: A Major Cause of Amplified Nitrate in River Water. *Sci. Total Environ.* **2016**, *548–549*, 173–188. [CrossRef]
8. Meimei, W.; Zizhen, J.; Tengbiao, L.; Yongchun, Y.; Zhuo, J. Analysis on Absolute Conflict and Relative Conflict of Land Use in Xining Metropolitan Area under Different Scenarios in 2030 by PLUS and PFCI. *Cities* **2023**, *137*, 104314. [CrossRef]
9. Iojă, C.I.; Niţă, M.R.; Vânău, G.O.; Onose, D.A.; Gavrilidis, A.A. Using Multi-Criteria Analysis for the Identification of Spatial Land-Use Conflicts in the Bucharest Metropolitan Area. *Ecol. Indic.* **2014**, *42*, 112–121. [CrossRef]
10. Milczarek-Andrzejewska, D.; Zawalińska, K.; Czarnecki, A. Land-Use Conflicts and the Common Agricultural Policy: Evidence from Poland. *Land Use Policy* **2018**, *73*, 423–433. [CrossRef]
11. Karimi, A.; Brown, G. Assessing Multiple Approaches for Modelling Land-Use Conflict Potential from Participatory Mapping Data. *Land Use Policy* **2017**, *67*, 253–267. [CrossRef]
12. Zou, L.; Liu, Y.; Wang, J.; Yang, Y.; Wang, Y. Land Use Conflict Identification and Sustainable Development Scenario Simulation on China's Southeast Coast. *J. Clean. Prod.* **2019**, *238*, 117899. [CrossRef]
13. Liu, J.; Liu, Y.; Li, Y. Classification evaluation and spatial-temporal analysis of "production-living-ecological" spaces in China. *Acta Geogr. Sin.* **2017**, *72*, 1290–1304.
14. Yang, Q.; Duan, X.; Wang, L.; Jin, Z. Land Use Transformation Based on Ecological-production-living Spaces and Associated Eco-environment Effects: A Case Study in the Yangtze River Delta. *Sci. Geogr. Sin.* **2018**, *38*, 97–106.
15. Kalabamu, F.T. Land Tenure Reforms and Persistence of Land Conflicts in Sub-Saharan Africa—The Case of Botswana. *Land Use Policy* **2019**, *81*, 337–345. [CrossRef]
16. Brown, G.; Raymond, C.M. Methods for Identifying Land Use Conflict Potential Using Participatory Mapping. *Landsc. Urban Plan.* **2014**, *122*, 196–208. [CrossRef]
17. Jiang, S.; Meng, J.; Zhu, L.; Cheng, H. Spatial-Temporal Pattern of Land Use Conflict in China and Its Multilevel Driving Mechanisms. *Sci. Total Environ.* **2021**, *801*, 149697. [CrossRef]
18. Long, H. Theorizing Land Use Transitions: A Human Geography Perspective. *Habitat Int.* **2022**, *128*, 102669. [CrossRef]
19. Zhang, Z.; Wang, X.; Wen, Q.; Zhao, X.; Liu, F.; Zuo, L.; Hu, S.; Xu, J.; Yi, L.; Liu, B. 2016. Research progress of remote sensing application in land resources. *J. Remote Sens.* **2016**, *20*, 1243–1258.
20. Journal of Geoinformation Science Editorial Department. "Spatial and Temporal characteristics of Land use/Cover Change in China in the New Era and its ecological and environmental Effects" column introduction. *J. Geo Inf. Sci.* **2017**, *19*, 1.
21. Zhang, L.; Zhao, J.; Chen, G.; Lin, Y.; Liu, F.; Peng, S. Impact of land use change on the value of ecosystem services based on SDG 15.3.1. *J. Soil Water Conserv.* **2024**, *38*, 268–277.

22. Kelly-Fair, M.; Gopal, S.; Koch, M.; Pancasakti Kusumaningrum, H.; Helmi, M.; Khairunnisa, D.; Kaufman, L. Analysis of Land Use and Land Cover Changes through the Lens of SDGs in Semarang, Indonesia. *Sustainability* **2022**, *14*, 7592. [CrossRef]
23. Dong, L. China's Renewed Perception of Global Environmental Governance. *Chin. J. Popul. Resour. Environ.* **2020**, *18*, 319–323. [CrossRef]
24. Calvert, K.; Mabee, W. More Solar Farms or More Bioenergy Crops? Mapping and Assessing Potential Land-Use Conflicts among Renewable Energy Technologies in Eastern Ontario, Canada. *Appl. Geogr.* **2015**, *56*, 209–221. [CrossRef]
25. Chen, Y.; Su, X.; Wang, X. Spatial Transformation Characteristics and Conflict Measurement of Production-Living-Ecology: Evidence from Urban Agglomeration of China. *Int. J. Environ. Res. Public Health* **2022**, *19*, 1458. [CrossRef]
26. Kim, I.; Arnhold, S. Mapping Environmental Land Use Conflict Potentials and Ecosystem Services in Agricultural Watersheds. *Sci. Total Environ.* **2018**, *630*, 827–838. [CrossRef]
27. Liao, L.; Dai, W.; Chen, J.; Huang, W.; Jiang, F.; Hu, Q. Spatial conflict between ecological-production-living spaces on Pingtan Island during rapid urbanization. *Resour. Sci.* **2017**, *39*, 1823–1833.
28. Niu, H.; Wang, J.; Jing, Z.; Liu, B. Identification and Management of Land Use Conflicts in Mining Cities: A Case Study of Shuozhou in China. *Resour. Policy* **2023**, *81*, 103301. [CrossRef]
29. Pan, F.; Wan, Q.; Zeng, J.; Wang, H.; Huang, Q. Evolution Characteristics and Influence Factors of Spatial Conflicts Between Production-Living-Ecological Space in the Rapid Urbanization Process of Hubei Province, China. *Econ. Geogr.* **2023**, *43*, 80–92.
30. Min, J.; Wang, R.; Liu, C. Spatiotemporal evolution of production-living-ecological spaces in the Aksu region. *J. Agric. Resour. Environ.* **2024**, *13*, 1319.
31. Zheng, W.; Guo, B.; Su, H.; Liu, Z. Study on Multi-Scenarios Regulating Strategy of Land Use Conflict in Urban Agglomerations under the Perspective of "Three-Zone Space": A Case Study of Harbin-Changchun Urban Agglomerations, China. *Front. Environ. Sci.* **2024**, *11*, 1288933. [CrossRef]
32. Wang, Z.; Zhang, J.; Li, H.; Su, W. Multi-scale spatio-temporal evolution and multi-scenario simulation of land use conflict in Chongqing. *Acta Ecol. Sin.* **2024**, *44*, 1024–1039.
33. Feng, Y.; Bi, R.; Wang, J.; Lv, C.; Zhang, Q. Spatial Conflict of Land Use Caused by Mining Exploitation and Optimal Allocation Scheme of Land Resources in River Basin. *China Land Sci.* **2016**, *30*, 32–40+2.
34. Wang, Y.; Li, P.; Li, W.; Zeng, X.; Xue, B. Mitigation Mechanism of Land Use Conflicts Based on Evolutionary Game: A Case Study of Shenfu New Area. *China Land Sci.* **2021**, *35*, 87–97.
35. Bao, W.; Yang, Y.; Zou, L. How to Reconcile Land Use Conflicts in Mega Urban Agglomeration? A Scenario-Based Study in the Beijing-Tianjin-Hebei Region, China. *J. Environ. Manag.* **2021**, *296*, 113168. [CrossRef]
36. Chen, L.; Zhang, A. Identification of Land Use Conflicts and Dynamic Response Analysis of Natural-Social Factors in Rapidly Urbanizing Areas—A Case Study of Urban Agglomeration in the Middle Reaches of Yangtze River. *Ecol. Indic.* **2024**, *161*, 112009. [CrossRef]
37. Sun, P. Temporal and Spatial Evolution of Land Use Conflicts in the Poverty Belt around Beijing and Tianjin from the Perspective of Ecological Security. Doctoral Thesis, China Agricultural University, Beijing, China, 2017.
38. Wang, C.; Wang, H.; Wu, J.; He, X.; Luo, K.; Yi, S. Identifying and Warning against Spatial Conflicts of Land Use from an Ecological Environment Perspective: A Case Study of the Ili River Valley, China. *J. Environ. Manag.* **2024**, *351*, 119757. [CrossRef]
39. Gao, Z.; Ye, J. Eco-environmental effects and differentiation mechanism of land use transition in Manas River Basin: A perspective based on the dominant function of "production-living-ecological" spaces. *Arid. Land Geogr.* **2024**, *47*, 1947–1956.
40. Liu, X.; Li, X.; Zhang, Y.; Wang, Y.; Chen, J.; Geng, Y. Spatiotemporal Evolution and Relationship between Construction Land Expansion and Territorial Space Conflicts at the County Level in Jiangsu Province. *Ecol. Indic.* **2023**, *154*, 110662. [CrossRef]
41. Wan, J.; Liu, Y.; Zhang, X. Conflict in Informal Rural Construction Land Transfer Practices in China: A Case of Hubei. *Land Use Policy* **2021**, *109*, 105573.
42. Zhou, D.; Zhao, X.; Li, P.; Jin, F.; Li, S.; Li, H.; Wang, J. Assessing Territorial Space Conflicts in the Coastal Zone of Wenzhou, China: A Land-Sea Interaction Perspective. *Sci. Total Environ.* **2024**, *926*, 171826. [CrossRef] [PubMed]
43. Wang, D.; Huang, L.; Chen, Z. Evolution of productional-living-ecological space and land use relative conflict at Nanchang County of Nanchang City from 2000 to 2020. *Bull. Soil Water Conserv.* **2024**, *44*, 426–436+445.
44. Hui, E.C.M.; Bao, H. The Logic behind Conflicts in Land Acquisitions in Contemporary China: A Framework Based upon Game Theory. *Land Use Policy* **2013**, *30*, 373–380. [CrossRef]
45. Pacheco, F.a.L.; Varandas, S.G.P.; Sanches Fernandes, L.F.; Valle Junior, R.F. Soil Losses in Rural Watersheds with Environmental Land Use Conflicts. *Sci. Total Environ.* **2014**, *485*, 110–120. [CrossRef] [PubMed]
46. Tao, Q. Measurement and Simulation Prediction of Conflict Level of "Three Living Things" in Typical Karst Mountain Watersheds of Guizhou Province. Master's Thesis, Guizhou Normal University, Guiyang, China, 2024.
47. Lu, Q.; Sun, J.; Xiao, Y.; Zhu, S.; Zhu, G.; Liu, J.; Li, X.; Liu, H. The Progression Traits of Spatial Conflicts within the Production–Living–Ecological Space among Varying Geomorphological Types of Mountain–Basin Areas in Karst Regions, China. *Ecol. Indic.* **2024**, *166*, 112324. [CrossRef]

48. Zuo, Q.; Zhou, Y.; Wang, L.; Li, Q.; Liu, J. Impacts of Future Land Use Changes on Land Use Conflicts Based on Multiple Scenarios in the Central Mountain Region, China. *Ecol. Indic.* **2022**, *137*, 108743. [CrossRef]
49. Fang, C.; Liu, H. The Spatial Privation and the Corresponding Controlling Paths in China's Urbanization Process. *Acta Geogr. Sin.* **2007**, *62*, 849–860.
50. Wang, J.; Liu, X. Recognizing and measuring spatial conflict of land use via "risk-effect". *Trans. Chin. Soc. Agric. Eng.* **2022**, *38*, 291–300.
51. Liang, X.; Guan, Q.; Clarke, K.C.; Liu, S.; Wang, B.; Yao, Y. Understanding the Drivers of Sustainable Land Expansion Using a Patch-Generating Land Use Simulation (PLUS) Model: A Case Study in Wuhan, China. *Comput. Environ. Urban Syst.* **2021**, *85*, 101569. [CrossRef]
52. Liang, X.; Liu, X.; Li, D.; Zhao, H.; Chen, G. Urban Growth Simulation by Incorporating Planning Policies into a CA-Based Future Land-Use Simulation Model. *Int. J. Geogr. Inf. Sci.* **2018**, *32*, 2294–2316. [CrossRef]
53. Hu, F.; Zhang, Y.; Guo, Y.; Zhang, P.; Lv, S.; Zhang, C. Spatial and temporal changes in land use and habitat quality in the Weihe River Basin based on the PLUS and InVEST models and predictions. *Arid. Land Geogr.* **2022**, *45*, 1125–1136.
54. Lin, Z.; Peng, S. Comparison of Multimodel Simulations of Land Use and Land Cover Change Considering Integrated Constraints-a Case Study of the Fuxian Lake Basin. *Ecol. Indic.* **2022**, *142*, 109254. [CrossRef]
55. Wang, B. Spatial-Temporal Pattern Evolution and Multi-Scenario Simulation of Land Use Conflict in Poyang Lake Area Based on PLUS Model. Master's Thesis, Jiangxi Normal University, Nanchang, China, 2023.
56. Zhang, X.; Gu, R. Spatio-temporal pattern and multi-scenario simulation of land use conflict: A case study of the Yangtze River Delta urban agglomeration. *Geogr. Res.* **2022**, *41*, 1311–1326.
57. Wang, B.; Shu, X.; Liao, F.; Li, Y.; Wan, Z. Spatitemporal of Land Use Conflicts and Multi-Scenario Simulationin Poyang Lake Area Based on Optimal Landscape Scale. *Res. Soil Water Conserv.* **2024**, *31*, 336–347.
58. Dong, G.; Ge, Y.; Jia, H.; Sun, C.; Pan, S. Land Use Multi-Suitability, Land Resource Scarcity and Diversity of Human Needs: A New Framework for Land Use Conflict Identification. *Land* **2021**, *10*, 1003. [CrossRef]
59. Yan, Z.; Li, W.; Wang, D. Outward Expansion or Networked Growth? Comparing Farmland Loss in Evolving Urban Agglomerations across Mollisol Regions in the Northern Hemisphere. *Cities* **2023**, *133*, 104106. [CrossRef]
60. Zhang, Y.; Li, J.; Pan, B. Evaluation and multi-scenario prediction of ecosystem services in the Yellow River Basin based on PLUS model: A case study of Shaanxi section. *Arid. Land Geogr.* **2024**, *47*, 1935–1946.
61. Li, W.; Yang, J.; Fu, B.; Zhao, Q.; Tan, Z.; Guan, X. Spatial-temporal changes and prediction of carbon storage in Greater Khingan Mountains based on PLUS-InVEST model. *J. Environ. Eng. Technol.* **2024**, *14*, 1892–1904.
62. Wang, D.; Zhang, C.; Wang, B.; Li, B.; Wang, Q.; Liu, D.; Wang, H.; Zhou, Y.; Shi, L.; Lan, F.; et al. Optimized CRISPR Guide RNA Design for Two High-Fidelity Cas9 Variants by Deep Learning. *Nat. Commun.* **2019**, *10*, 4284. [CrossRef]
63. Xie, H. Regional eco-risk analysis of based on landscape structure and spatial statistics. *Acta Ecol. Sin.* **2008**, *28*, 5020–5026.
64. Peng, Y.; Wang, J.; Wang, S.; Tian, L.; Liu, J.; Wu, Z. Spatiotemporal pattern evolution of land use conflict in Urumqi City from the perspective of ecological security. *Arid. Land Geogr.* **2024**, *47*, 81–92.
65. Zhou, Z.; Zhu, C. Recent Progress of Studies on the Regional Spatial Integration and Its Prospects in China. *Areal. Res. Dev.* **2009**, *28*, 1–5.
66. Mo, W.; Wang, Y.; Zhang, Y.; Zhuang, D. Impacts of Road Network Expansion on Landscape Ecological Risk in a Megacity, China: A Case Study of Beijing. *Sci. Total Environ.* **2017**, *574*, 1000–1011. [CrossRef] [PubMed]
67. Liu, B.; Guo, X.; Zhu, Y. Analysis of soil heavy metal sources in Jinzhong basin based on random forest model. *Arid. L. Resour. Environ.* **2019**, *33*, 106–111.
68. Xu, H. A remote sensing urban ecological index and its application. *Acta Ecol. Sin.* **2013**, *33*, 7853–7862.
69. Cai, L.; Tang, X. Multi-scenario Simulation of Production-Living-Ecological Space and Carbon Storage Assessment in Ecological Transition Zone: A Case Study of Gansu Province. *Chin. J. Environ. Sci.* **2024**, 1–19. [CrossRef]

Disclaimer/Publisher's Note: The statements, opinions and data contained in all publications are solely those of the individual author(s) and contributor(s) and not of MDPI and/or the editor(s). MDPI and/or the editor(s) disclaim responsibility for any injury to people or property resulting from any ideas, methods, instructions or products referred to in the content.